UNIVERSITAT POLITÈCNICA DE CATALUNYA

Chemical Engineering Department

Ph. D. Program: Chemical Process Engineering

CHARACTERIZATION AND MODELLING OF MICRO AND NANOFLUIDIC SYSTEMS

Thesis presented by Edxon Eduardo Licon Bernal in order to obtain the Ph. D. degree from the *Universitat Politècnica de Catalunya* inside the program of Chemical Process Engineering.

Barcelona, February 2015

Thesis Advisor:
Ph. D. Andriy Yaroshchuk

Nature is the source of all true knowledge. She has her own logic, her own laws, she has no effect without cause nor invention without necessity.
Leonardo da Vinci

Acknowledgements

This work would not have come to fruition without the help of my advisor, the Professor Andriy Yaroshchuk, who besides being an excellent scientist, is an extraordinary human being. His extensive experience and creativity to solve any problems make me feel a deep respect and admiration for him. He put his skills to my service and shared with me his way of seeing the world, I will always be grateful.

Emil Zholkovskiy and Volodymyr Kovalchuk are other great teachers with whom I spent hours and hours of discussions and approaches. Beyond the opportunity to learn from them at the professional level, I appreciate the sincere friendship and all the attentions they have had to me the whole time.

I also thank José Luis Cortina and Cesar Valderrama for including me in their research group the last months of the thesis. It gave me the opportunity to apply my skills in various subjects and opened several growth opportunities for me. In particular, interact as supervisor of students and help them to make their dissertation works made me realize how rewarding a scientific career can be.

Thanks for the financial support of my studies to the National Council of Science and Technology of Mexico (CONACYT) and to the Education, Audiovisual and Culture Executive Agency of the European Union (EACEA).

I make a special mention of my family, because each and every one of them has been the foundations of what I am. Since childhood my parents instilled me to question everything, unwittingly, they awakened in me the love for learning.

I especially want to thank my beautiful wife, Dalia, and my lovely children, Edu and Eva, for being by my side every time. This work belongs to them as much or more than to me; Feel proud about this achievement since we have accomplished it together.

Since they are too many for mention them here, my humble recognition to all the people who contributed in any way for making this work.

Agradecimientos

Este trabajo no hubiese llegado a buen término sin la ayuda de mi director de tesis el Dr. Andriy Yaroshchuk, quien además de ser un excelente científico, es un extraordinario ser humano. Su amplia experiencia y creatividad para resolver cualquier tipo de problema hacen que sienta por él un profundo respeto y admiración. Puso sus aptitudes a mi servicio y me compartió su manera de ver el mundo, siempre le estaré agradecido.

Emil Zholkovskiy y Volodymyr Kovalchuk son otros grandes maestros con los que pasé horas y horas de discusiones y planteamientos. Más allá de la oportunidad de aprender de ellos en el plano profesional, les agradezco su amistad sincera y todas las atenciones que han tenido hacia mí durante todo este tiempo.

Agradezco también a José Luis Cortina y Cesar Valderrama el haberme incluido en su grupo de investigación en la parte final de la tesis. Brindarme la oportunidad de aplicar mis capacidades en diversos temas me abrió muchas ventanas de crecimiento. En especial, interactuar con estudiantes y ayudarles a realizar sus trabajos finales me hizo darme cuenta cuan gratificante puede ser una carrera científica.

Gracias por el apoyo económico para la realización de mis estudios al Consejo Nacional de Ciencia y Tecnología de México (CONACYT) y a la Agencia ejecutiva de educación, audiovisual y cultura de la Unión Europea (EACEA)

Hago una mención especial a mi familia, porque todos y cada uno han representado mis pilares en todo momento. Desde pequeño mis padres que me inculcaron a cuestionarlo todo, sin darnos cuenta despertaron en mí el amor por aprender.

Sobre todo quiero agradecer a mi hermosa esposa, Dalia, y a mis cariñosos hijos, Edu y Eva, por estar a mi lado cada momento. Este trabajo les pertenece tanto o más que a mí; siéntanse orgullosos de que este logro lo hemos alcanzado juntos.

En general pero sin demeritar, a todas las personas que contribuyeron de alguna manera en la realización de este trabajo, mi humilde reconocimiento.

Abstract

Lab-on-a-chip arrangements are ever more frequently used for the miniaturization of chemical and biochemical analysis. In these arrangements, all the manipulations of analyte transport, separation, mixing with reactants and detection are integrated and implemented at the scale of a microchip of several cm in size. This makes possible a dramatic reduction in the required amounts of analytes and reactants, as well as in the time of analysis. Besides that, automation and high-throughput operations (due to parallelization) become much easier than in the conventional “macro-laboratory” environments.

A basic element of a micro-analytical system is a micro-channel. The regularities of volume and solute transfer (electrically- and pressure-driven) in micro-channels are a subject matter of microfluidics. These regularities have been extensively studied both experimentally and theoretically over the last two decades. In recent 5 years, an ever increasing attention has being paid to nanofluidics, which deals with equilibrium and transport phenomena in channels whose dimensions are comparable with the so-called Debye screening length (1 to 30 nm, depending on the ionic strength of the buffer solution). It has been demonstrated that the use of nano-fluidic elements, for example, makes possible a very strong (orders of magnitude) pre-concentration of analytes before their further manipulation in micro-analytical systems.

To be practically useful, nanofluidic elements have to be connected to micro-fluidic ones through nano-/micro-interfaces. One of the characteristic features of such interfaces is their current-induced concentration polarization. In this process, the concentration of buffer solution can strongly decrease in the micro-channel close to its interface with the nano-channel(s) or nano-porous media. This decrease in the concentration brings about a considerable increase in the local rate of electro-osmosis, and this, in turn, causes a vigorous electrokinetic mixing, which strongly affects the phenomenon of concentration polarization itself. Therefore, there is a strong non-linear coupling between the concentration polarization and electro-osmosis, which has to be understood to make possible the optimization of applications of micro and nanofluidic systems.

According to the great interest in the development of new porous materials including their subsequent integration into biomedical devices and industrial applications, the description of the characteristics of nanoporous media (for example membranes) and the development of characterization techniques are crucial for controlling the behavior of systems that include separation and purification processes with such technologies.

Within this thesis various developments in the field of microfluidics, separation and purification of substances has been carried out: For the field of microfluidics, this study may be useful for the description of the first stages of the concentration polarization in microfluidic systems coupling membrane technology or micro/nano interfaces. Furthermore, it was shown that for such systems, Taylor-Aris theory is applicable locally in large open microchannels within a range of Peclet numbers. Furthermore, it was possible to derive a simple analytical approach for internal concentration gradient within long channels in terms of only a few parameters, determined numerically. This approach is useful for developing future experimental studies.

In equipment used for measuring the zeta potential of porous media, the variation in the channel height is technically possible. This thesis shows that under such conditions, the fluid flow can become undeveloped turbulent, which provokes that conventional approaches to the interpretation of electrokinetic measurements should be changed accordingly. A mathematical model for arbitrary electrolytes mixtures has been defined to describe the transport phenomena occurring in several osmotic separation processes. The limited number of adjustable parameters contained in this model makes possible its unequivocal determination from a limited set of experimental data.

According to the results of this work, hollow fibers membrane contactors are useful as a polishing step for removing low levels of ammonia in water. It has been determined and validated experimentally a mathematical model which helps to describe the influence of operating conditions, such as flow, ammonia concentration and pH of the system for both configurations, closed and open loop. These results are important for designing production systems of ultrapure water that can be used in the production of hydrogen by water electrolysis.

The application of microfluidics technologies at industrial scale is one of the main challenges faced on this knowledge field; however, there are some devices that are already being used systematically at industrial level for separation purposes that fulfil the criteria for being considered within that group of technologies. Such is the case of hollow fiber membrane contactors. This thesis establishes patterns and basic concepts that can serve as basis for the characterization and description of miniature versions of well-known separation processes, which in turn, can be used for the development of processes in new biochemical applications.

Resumen

La miniaturización de los análisis químicos y bioquímicos está cada vez utiliza más utilizada. Todas las manipulaciones de transporte de las muestras, la separación, la mezcla con los reactivos y la detección se integren y apliquen a escala de un microchip de varios centímetros de tamaño. Esto hace posible una reducción dramática en las cantidades requeridas de muestra y reactivos, así como en el tiempo del análisis. Además de eso, las operaciones de automatización y de alto rendimiento (debido a la paralelización) se vuelven mucho más fáciles que en los entornos convencionales "macro-laboratorio".

Un elemento básico de un sistema de micro-analítico es un canal de micro. Las regularidades de transferencia de volumen y soluto (eléctricamente y accionado por presión) en micro-canales son un tema de microfluidos. Estas regularidades se han estudiado ampliamente experimental y teóricamente en las últimas dos décadas. En los últimos 5 años, ha de ser pagado una atención cada vez mayor a nanofluidos, que se ocupa de fenómenos de equilibrio y de transporte en los canales cuyas dimensiones son comparables con el grosor de la doble capa eléctrica (1 a 30 nm, dependiendo de la fuerza iónica del tampón solución). Se ha demostrado que el uso de dichos elementos hace posible fuertes pre-concentraciones de las muestras antes de su manipulación en sistemas de analíticos. Para ser útil en la práctica, los elementos nanofluídicos tienen que ser conectados a los microfluídicos a través de nano / micro-interfaces. Uno de los rasgos característicos de tales interfaces es su polarización de la concentración inducida por la corriente. En este proceso, la concentración de la solución tampón puede disminuir fuertemente en el micro-canal cerca de su interfaz con el canal nano (s) o medios de nano-poroso. Esta disminución en la concentración provoca un aumento considerable en la tasa local de electro-ósmosis, y esto, a su vez, causa una mezcla vigorosa electrocinética, que afecta fuertemente el fenómeno de la misma polarización de la concentración. Por lo tanto, hay un fuerte acoplamiento no lineal entre la polarización de la concentración y electro-ósmosis, que tiene que ser entendido para hacer posible la optimización de las aplicaciones de los sistemas de micro y nanofluídicos.

De acuerdo con el gran interés en el desarrollo de nuevos materiales porosos incluyendo su posterior integración en dispositivos biomédicos y aplicaciones industriales, la descripción de las particularidades de los medios nanoporosos (por ejemplo membranas) y el desarrollo de técnicas de caracterización son cruciales para controlar el comportamiento de los sistemas que incluyen procesos de separación y purificación con dichas tecnologías. En esta tesis se han llevado a cabo diferentes avances en el campo

de la microfluídica, la separación y purificación de sustancias: Para el campo de la microfluídica, este estudio puede ser útil para la descripción de las primeras etapas de la polarización en los sistemas microfluídicos que acoplan tecnología de membranas o micro/nano interfaces. Por otro lado, se demostró que para tales sistemas, la teoría de Taylor-Aris es aplicable localmente dentro de microcanales abiertos en una amplia gama de números de Péclet. Además, fue posible derivar una aproximación analítica sencilla para el gradiente de concentración interno dentro de canales largos en términos de sólo unos pocos parámetros, determinados numéricamente. Esta aproximación es útil para desarrollar futuros estudios experimentales. En algunos equipos usados para la medición del potencial zeta de medios porosos, la variación de la altura del canal es técnicamente posible. En el presente documento se muestra que en estas condiciones, el flujo de fluido puede llegar a ser de transición a turbulento y los enfoques convencionales para la interpretación de las mediciones electrocinéticas debe modificarse en consecuencia. Se definió un modelo matemático que permite describir de manera sencilla, fenómenos de transporte que ocurren en diversos procesos de separación osmóticos, para mezclas de electrolitos arbitrarias. El número limitado de parámetros ajustables que contiene este modelo hace factible su determinación inequívoca a partir de un conjunto limitado de datos experimentales. De acuerdo con los resultados de esta tesis, los contactores de membrana con fibras huecas son útiles como etapa de pulido para la eliminación de bajos niveles de amonio en agua. Se ha determinado y validado experimentalmente un modelo matemático el cual ha ayudado a describir la influencia de las condiciones de funcionamiento, tales como flujo, concentraciones de amonio y pH del sistema para ambas configuraciones, de lazo cerrado y abierto. Dichos resultados son útiles para el diseño de sistemas de producción de agua ultra pura que puede ser usada en la producción de hidrogeno por electrolisis.

La aplicación de las tecnologías de microfluidos a escala industrial es uno de los principales retos que enfrentar en este campo del conocimiento; sin embargo, existen algunos dispositivos que ya se están utilizando de forma sistemática a nivel industrial para fines de separación que cumplen criterios necesarios para considerarlos dentro del grupo de las tecnologías de microfluídica. Tal es el caso de los contactores de membrana de fibra hueca. Acotando a los resultados presentados en microfluídica, con este trabajo se han establecido patrones y definido conceptos básicos, dentro de este campo de la ciencia, que pueden servir como bases en la caracterización y la descripción de versiones en miniatura de procesos de separación bien conocidos, los cuales se pueden usar para el desarrollo de procesos en nuevas aplicaciones bioquímicas.

Index

Introduction

This Chapter includes a review of the major contributions made previously to the topics covered in this Thesis. Moreover, concepts with special interest will be illustrated.

1.1 Micro- and nanotechnologies

Micro- and nanotechnologies have significant impacts on the development of new products and on the production of technologies. This emerging field includes the use of effects at such scales where unique phenomena enable novel applications. The continuous miniaturization and the corresponding increase in the density of integration is a challenge to the materials and processes in use.

Microsystems, including micro-electromechanical systems (MEMS), nano-electromechanical systems (NEMS), optical, electronic, and electrochemical microsystems, hold the promise of a new class of multifunctional devices and systems for many applications ranging from advanced computing, chemical and biological analysis and detection, drug delivery and discovery, tissue engineering, chemical and materials synthesis, to energy storage and conversion. New advanced micro-systems with integrated nanometre-scale structures and functions present a multidisciplinary challenge and the performance of such microsystems also depends on the understanding of the properties on both the nano- and microscales.

The nanotechnology comprises all products with a size of at least one component below 100 nanometres in one or more dimensions that makes physical, chemical or biological effects available which cannot be achieved above this dimension without a loss of performance. An overview of the effects and applications of the reduced dimensionality of nanomaterials is listed in the table 1.

Table 1. Effects of nanomaterials and applications due to the reduced dimension.

Effects	Applications
Higher surface to volume ratio, enhanced reactivity.	Catalysis, solar cells, batteries, gas sensors.
Lower percolation threshold.	Conductivity of materials.
Increased hardness with decreasing grain size.	Hard coatings, thin protection layers.
Narrower band gap with decreasing grain size.	Opto-electronics.
Higher resistivity with decreasing grain size.	Electronics, passive components, sensors.
Increased wear resistance.	Hard coatings, Tools.
Lower melting and sintering temperature.	Processing of materials, low sintering materials.
Improved transport kinetic.	Batteries, hydrogen storage.

It becomes so important during the last decade, that the United States government, the country which has invested more in this area, has spent nearly about 12 Billion dollars in research and development at 2010, since the foundation of the national nanotechnology initiative in 2000 year, with an increasing investment as shown in Figure 1.[1]

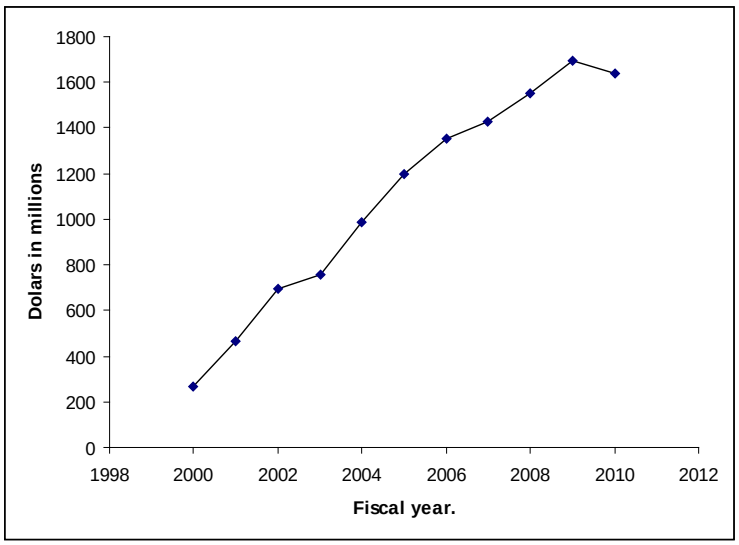

Figure 1. USA Budget of the last decade.[1]

Others countries have started their own nano-technological national programs after that. Japan and South Korea on 2001, the European community and Taiwan on 2002.[2] All of them having a budged greater than one hundred million dollars per year.

After several years, on 2007 a strategic plan of United States was taken in order to achieve four goals [3]:

1. Maintain a world-class research and development program aimed at realizing the full potential of nanotechnology.

2. Facilitate transfer of new technologies into products for economic growth, jobs, and other public benefit.

3. Develop educational resources, a skilled workforce, and the supporting infrastructure and tools to advance nanotechnology.

4. Support responsible development of nanotechnology.

The main countries are agree with this goals and support the idea that it is important that money spent has to be reflected in products that improve the users life quality. Research and innovation have been confirmed as key challenges in the 2002 Barcelona European Council, which set the goal of raising overall research investment in

the European Union (EU) from1.9% of gross domestic product (GDP) to around 3% by 2010. Nearly all Member States have set targets, which would bring research investment in the EU to 2.6% by 2010. But instead of rising, the overall level of EU research is currently more or less stagnant [4]. Nevertheless, is clear that a global aim has been established and it is important to concentrate all the efforts to achieve this goal.

Some of the goals of nanotechnology are: unlimited optimization of product properties in the field of power engineering (fuel cells, batteries, solar cells), environmental technology (resource cycles, waste management, cleaning), information technology (high-density storage, powerful processors), and in the sector of health. Those are the identified future markets that offer good opportunities for exploiting nanotechnology. For developing this technology a completely new set of metrology devices is needed.

The equipment for analytical or manipulatory purposes that allows controlled fabrication, movement or measurement resolution with a precision below 100 nanometres belongs to the group of this research and development field. For example the Lab-on-a-chip arrangements, which are ever more frequently used for the biochemical analysis, all the analyte manipulations of transport, separation, mixing with reactants and detection are integrated and implemented at the scale of a microchip of several centimetres in size. This makes possible a dramatic reduction in the required amounts of analytes and reactants, as well as in the time of analysis. Besides that, automation and high-throughput operations become much easier than in the conventional macro-laboratory environments due to the parallelization [5].

1.1.1 Microfluidics

A basic element of a micro-analytical system is a microchannel. The regularities of volume and solute transfer (electrically- and pressure driven) in microchannels are a subject matter of microfluidics, which is dedicated to miniaturized plumbing and fluidic manipulation and offers the possibility of solving outstanding system integration issues for biology and chemistry by allowing automation to proceed to scales that will rival electronic integrated circuits.[6] These regularities have been extensively studied both experimentally and theoretically over the last two decades [7].

1.1.2 Nanofluidics

In recent years, an ever increasing attention has being paid to nanofluidics, which deals with equilibrium and transport phenomena in channels whose dimensions are comparable with the electrical double layer, (so-called Debye screening length), which has a size of 1 to 30 nm, depending on the ionic strength of the buffer solution. The aim of this

rapidly growing domain is to accurately control fluidic motion and molecular motion at the nanometre scale and to transform this knowledge in applicable devices [8].

To be practically useful, nanofluidic elements have to be connected to microfluidic ones through nano-/micro-interfaces. Fluid flow at the nanometre-scale has been implicitly studied in many classical disciplines for decades. The knowledge that has been acquired in these disciplines is important for nanofluidics and has to be considered. The reason why nanofluidics has only recently received its name is due to the rise of microfluidics in the 1990s and the advent of nanoscience and nanotechnology [8].

A surface that bears a charge, positive or negative, in contact with a liquid develops a shielding layer containing counterions which is created within the liquid near the surface. The shielding layer thickness is indirectly proportional to the salt concentration. An important ratio to characterize fluid flow in nanochannels is the quotient of the nanopore radius over the shielding layer thickness. When these two parameters are comparable in size, a nanochannel becomes counterion selective.

It has been demonstrated that the use of nanofluidic elements, for example, makes possible analytes pre-concentration of several orders of magnitude, before their further manipulation in micro-analytical systems.[9] Besides that, it has been shown that in nano-channels, one can achieve electrophoretic separation of analytes according to their charges, which is not possible in micro-channels [10-11].

Furthermore, with the available technology some well defined nanochannels have been developing in order to study nano-/micro-interfaces [12,13]. Nevertheless, other materials like nano-porous membranes, gels or polymers have been used with this and other proposes [14].

One of the characteristic features of such interfaces is their current-induced concentration polarization. In this process, the concentration of buffer solution can strongly decrease in the micro-channel close to its interface with the nano-channel(s) or nano-porous media. This decrease in the concentration brings about a considerable increase in the local rate of electro-osmosis and thus in turn, causes a vigorous electrokinetic mixing, which strongly affects the phenomenon of concentration polarization itself [15, 16]. Therefore, there is a strong non-linear coupling between the concentration polarization and electro-osmosis, which has to be understood to make possible the optimization of applications of nanofluidic systems.

These phenomena have already been observed experimentally but the reported experimental systems have typically quite complicated geometries, which made a

quantitative interpretation difficult. The theoretical models used have also been complex and often deficient [16].

1.2 Membranes:

Commercially, membrane filtration bears a great acceptance as an important step in many of the process in several industries, as well as in water purification.[17] Very specific separations have been obtained at ambient temperature with no phase change which makes membrane filtration a cost-effective separation method compared to others such as centrifugal separation, vacuum filtration, and spray drying. The hydrostatic pressure is most often the driving force, but can also be electrical potential, concentration gradient, or temperature.

In biotechnology, this technology is applied in bioseparation and hemodialysis, where blood of uremia patients is purified against a physiological saline solution, which is necessary to prevent the transfer of vital non-toxic low molecular solutes such as potassium or sodium [18].

Nowadays, the last important application of membranes is electrochemical cells, for which ion exchange membranes have specially been researched and developed. These membranes have found use in energy generation (fuel cells), effluent treatment, and recycling. Ongoing research in batteries theoretically has shown that their efficiency can be maximized at a specific ionic strength of the solution [19-21].

The filtering processes can be ordered with decreasing pore diameter (from 4 μm up to 1 nm) as: microfiltration, ultrafiltration, nanofiltration, reverse osmosis and gas separation.

Microfiltration. The separation of solid from liquid is carried out by mechanical means of sieving. It only retains suspended solids, while proteins pass the membrane. In microfiltration the pressure driven feed flow is widely applied perpendicular to the membrane surface and the retained particles accumulate on the surface. This problem is called fouling and in this case, can be reduced by the use of tangential flow, in which the feed stream flows along to a membrane surface and thus permeating species pass through the membrane [22].

Ultrafiltration. The application of ultrafiltration is the separation of macromolecules. Proteins and suspended solids are rejected by ultrafiltration, while smaller components such as solvents and salts pass through. In combination with microfiltration it is very often used to solve any separation problem, involving particulate material and macromolecules [23].

Nanofiltration. Depending on the shape and size of the molecules, uncharged, dissolved materials, and organic compounds are retained by pressure driven nanofiltration. It rejects only ions with more than one charge [24].

Gas separation. Gas permeation uses homogenous membranes which separate species in terms of diffusivity and concentration in the membranes. This membrane technology has only recently been commercially applied to separate individual components from mixtures of gases. The membranes are non-porous thin layers on porous substrates and some of them take advance of its hydrophobicity for transfer for example gases between two liquid phases without placing them in direct contact [24].

Reverse osmosis. Membranes with the smallest available pores are used worldwide in reverse osmosis. This process allows removing particles as small as ions from a solution. Reverse osmosis is mainly used to purify water because the semi-permeable membrane rejects bacteria, salts, sugars, proteins, particles, dyes, radioactive and hazardous metal cations, and other constituents from contaminated water[22]. It is called reverse osmosis because water is forced by pressure in the opposite direction to the equilibrium-driven osmotic flux.

Membranes having a similar size of pores such as in reverse osmosis are also used in electrodialysis, but here the membranes are electrically charged and therefore selectively remove ions. Instead of applying a hydrostatic pressure, an electrical potential is used as the driving force for desalting foods and water. The economic advantage gained with electrodialysis is the specificity and efficiency of separation achieved at low temperatures [23].

To explain the reverse osmosis as simple as possible, picture out a system composed of two reservoirs *I* and *II* connected by a semi-permeable membrane. If both reservoirs are filled with water (Figure 2), there is no level difference *H*.

When solute is added to a reservoir I (Figure 1-2b) an osmotic pressure results creating a flow from reservoir II to I. The system is stabilized when the osmotic pressure is equal to the hydrostatic pressure given by

$$cRT = g\rho_m H \quad (1)$$

where: c is the molar solute concentration, R is the gas constant, and T is the absolute temperature, g is the gravitational acceleration, and ρ_m is the water specific gravity.

In reverse osmosis, the equilibrium driven osmotic flow from reservoir *II* to *I* is reversed by applying an external pressure P (i.e. 10 – 100 bar) on the side of higher concentration (reservoir *I*).

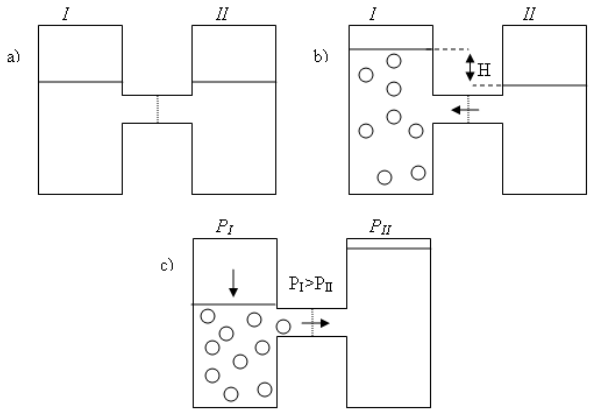

Figure 2. Illustration of osmosis and reverse osmosis.

1.2.1 Problems with the membranes at micro-scales

Membranes are very versatile in use, but there will be challenges besides the traditional sealing issues. The next three challenges might be encountered to apply them to micro- and nanofluidics [7]:

1. *The issue of concentration polarization.*

In concentration polarization, the removal rate of to solvent from to solution through to membrane is faster than the transport of new solvent from the bulk to the membrane surface. As result, an increased concentration of solute at one side of the membranes, leads to decrease in effective driving force over them. Vigorous mixing at the membrane surface, in order to reduce the thickness of the concentration polarization layer, is induced at macroscale to solve this. However, in the laminate regime of microfluidics, this degree of mixing is not achievable.

2. *The Fouling of the membrane.*

It depends directly on impurities and on interactions between components in the feed and the membrane. Then it would be necessary to prefilter all solutions before entering to chip. Another approach is to use membranes in disposable devices.

3. *The pressure driving force.*

For microfluidic chips the assumption of a pressure difference constant along the membrane may not be valid. Since the channel dimensions approach the pore dimensions of the membrane. Therefore, the driving force may vary in the channel directions, leading to a difference in local performance.

1.2.1 Integrated nanoporous membranes

Kuo et al [25] monitored electrokinetic transport of charged dyes to investigate the flow control, integrating a nanoporous membrane in a three-dimensional hybrid

microfluidic and nanofluidic system. The net fluid flow could be controlled through a polycarbonate nuclear track-etched membrane which was sandwiched between two microchannels made in Polydimethylsiloxane (PDMS). It shows the interest in making use of nanometre-sized apertures for micro total analysis systems (μTAS), which with the lab-on-a-chip devices, both aim at integrating all steps of biochemical analysis on one microchip [26,27] .

As biological and medical applications mostly use liquids and small sampling volumes, microfluidic devices are in general well adopted to perform analysis and other operations in this field. The big size of the above mentioned industrial membrane filtration systems is not compatible with their integration in biomedical devices.

Recently, μTAS has gained further expansion in two domains. The first one is in cell-based systems [28]. Growth of attached and suspended cells in microfluidic systems and the development of tissue cultures on chip are being investigated. The second domain in μTAS which has gained increased emphasis are new approaches to pre-concentrate and separate proteins and DNA molecules. Charge selectivity of nanofluidic structures can become a major tool for genomic and proteomic μTAS. Although the effort to develop μTAS is outstanding, their commercial impact is still very small.

IMEDD Inc. proposed a prototype of a small nanoporous implant, designed for constant level diffusion of drug through a nanochannel membrane [29, 30]. This device has the advantage of assures medical treatments over long periods with no additional interferences.

1.3 Phenomena at micro-/nano Interfaces

1.3.1 Concentration polarization

The phenomenon of concentration polarization (CP) is caused by the difference in the transport numbers of ions between two adjacent media, for example, on the boundary between an ion-exchange membrane and an aqueous electrolyte solution when applying a pressure or electric driving force in order to purify water.

When an external electric field is applied across a nanochannel, current transport is superimposed to diffusion. This ionic transport can induce considerable forces on electrolytes in nanometre-sized apertures due to which convection has to be considered [31]. The results are concentration polarization at the nanochannel interface and limiting current densities which are described in literature and discussed subsequently. In solution the electric current is carried by both cations and anions and their transference numbers (fraction of current carried by a certain ion) are about equal.

However, in an ion-selective nanochannel current is mainly transported by the counterions resulting in a transference number close to 1. At the anodic side of a cation-selective nanochannel (see Figure 3) the concentration of ions in the solution is reduced because of the lower transport number of cations in the solution than in the nanometre-sized aperture [32]. Anions move in opposite direction and cannot be compensated by the few anions that remain in the nanochannel. Because of electroneutrality, cations and anions are reduced by the same amount in front of the nanochannel on the anodic side where a concentration gradient is established.

At the other side of the nanochannel facing the cathodic side there occurs an accumulation of cations because more cations are transferred through the nanochannel than can be carried away by the electric current [32]. The transference number of anions in the nanochannel is almost zero and therefore they get accumulated at the cationic side of the nanometre-sized aperture [33]. Electroneutrality has to be fulfilled in this enriched zone of ions.

The depletion and accumulation of ions at the nanochannel interface by the electrical current is referred to as concentration polarization. This situation is presented in Figure 3 where cations are mainly transported by the migrational flux J_{ca}^{mig} in the nanometre-sized aperture. Anions are more or less excluded and their flux through the nanochannel compared to the one of cations is small. Diffusion of both, cations and anions, which are denoted as salt, result in the diffusional salt flux J_s^{diff} through the nanochannel from the concentrate towards the dilute side. Also J_s^{diff} is much smaller than J_{ca}^{mig}. In the convective-diffusion boundary layers (CDL) at both sides of the nanometer-sized aperture cations and anions are transported by the migrational fluxes J_{ca}^{mig} and J_{an}^{mig}, but in different directions which generates a concentration gradient. This concentration gradient leads to a diffusional flux of salt J_s^{diff}, which is towards the nanochannel on the dilute side and towards the bulk solution on the concentrate side of the nanochannel following the concentration gradients in the CDL.

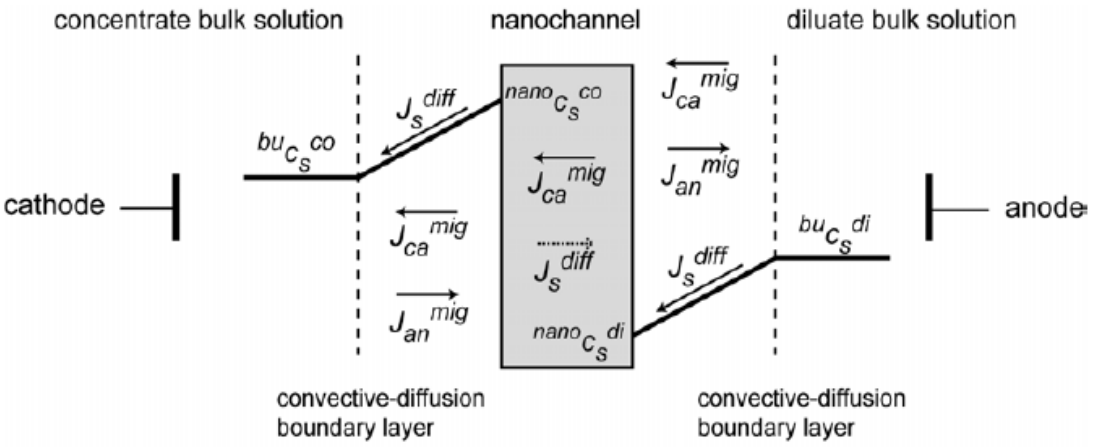

Figure 3. Schematic drawing illustrating the concentration polarization at nanochannel interfaces.[32]

In the Figure 3 concentration profiles of salt in the convective-diffusion boundary layer on both sides of the cation-selective nanochannel are presented as well as the fluxes J of cations, anions, and salt in the CDL and in the nanochannel. The superscripts *mig* and *diff* refer to migration and diffusion, the superscripts *di* and *co* refer to dilute and concentrate solution, and the superscripts *bu* and *nano* refer to bulk phase and nanochannel interface, and the subscripts *an, ca*, and *s* refer to anion, cation, and salt.

1.3.2 Limiting current

Concentration polarization can lead to a high salt concentration on the cathodic side and if it exceeds solubility limits of the solution constituents, precipitation of salts may occur resulting in an additional electrical resistance. When, due to concentration polarization, on the anodic side of the nanochannel the salt concentration at the nanochannel interface is reduced to zero, there are no more salt ions available to carry the electric current. This results in a limited current I_{lim} which corresponds to region II in Figure 5. To calculate this limited current the electrochemical analog to Fick's first law is considered

$$I = nFAD^{*}D_x(c) \quad (3)$$

where *n* is the number of electrons transferred per molecule. The concentration gradient is commonly approximated by a linear extrapolation of the *c* versus *x* slope at *x* = 0 and is given by [34]

$$I = nFAD * (C_b - C(x=0))/ \delta \quad (3.1)$$

where C_b is the bulk concentration and δ is the convective-diffusion boundary layer (CDL) thickness which is present at solid-liquid interfaces [35]. The CDL is usually between 10 μm and 400 μm thick [36] and is shown in Figure 4 at an interface electrode - bulk solution. The concentration c(x=0) decreases to the bulk concentration *cb* within the

convective-diffusion boundary layer thickness δ. When studying transport through nanochannels, this aperture can be regarded as an electrode out of which current is spreading. This spreading current is determined by the geometric cross-section of the nanochannel [37, 38] and characterizes the CDL.

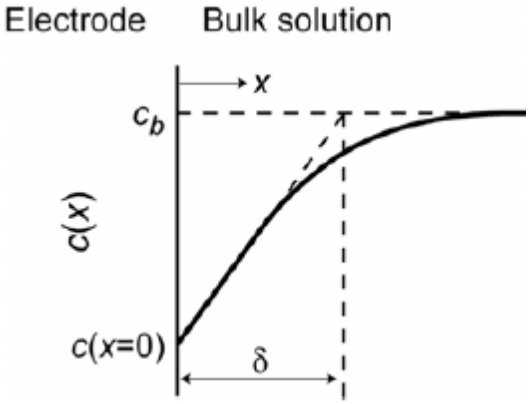

Figure 4. Schematic presentation of the concentration profile at the interface electrode – bulk solution.[41]

From Equation (3.1) it can be seen that a maximal current is obtained when $c(x = 0) = 0$, resulting in the limiting current [39]

$$I_{lim} = nFAD * Cb/ \delta \quad (3.2)$$

According to Equation (3.2) which is based on the classical picture of concentration polarization, the limiting current cannot be exceeded unless other ions than the salt ions become available for the transport of current in the salt depleted CDL. This is the case when water dissociation leads to the production of H^+ and OH^- ions, which will then carry the electric charges. This results in a so-called overlimiting current as presented in region III of Figure 5, which presents a typical voltage-current curve for a cation-exchange membrane. As a consequence, drastic pH value shifts with an increase of the pH value on the anodic side of the nanochannel and a decrease of the pH value on the cathodic side are obtained. In region I the current is increasing more or less linearly with the applied voltage according to Ohm's law. Due to concentration polarization a limiting current is observed in region II with the magnitude Ilim. The classical theory of concentration polarization predicts a true saturation of the voltage-current curve (dashed line), but other effects lead to overlimited currents in region III.

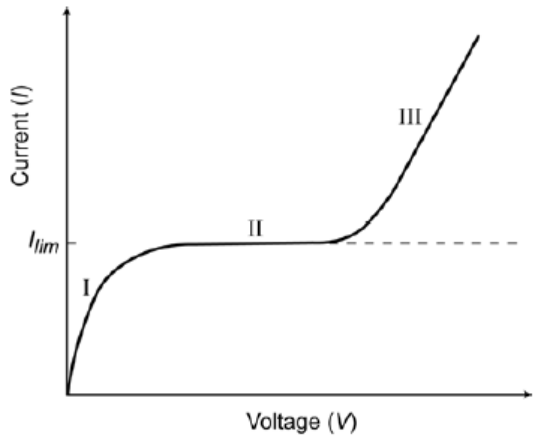

Figure 5. Scheme of a typical voltage-current curve of a cation-exchange membrane.[46]

1.3.3 Electrical double layer

Due to the fixed surface charge at the solid interface, an oppositely charged region of counterions develops in the liquid to maintain the electroneutrality of the solid-liquid interface. This screening region is denoted as the Electrical double layer (EDL), because ideally it consists of opposite charges, some of which are bound while others are mobile. The electrical double layer was initially represented by a simple capacitor, usually attributed to the model of Helmholtz. Guy and Chapman treated one layer of charge smeared uniformly over a planar surface immersed in an electrolyte solution. Stern introduced the Stern layer between the inner and outer Helmholtz planes, in which the charge and potential distribution are assumed to be linear, and a diffuse layer further from the wall where the Gouy-Chapman theory is applied. This model is presented in Figure 6, which is separated into three layers:

1. The *inner Helmholtz plane* and bears the potential Ψ_i, where co-ions and counterions are not hydrated and are specifically adsorbed to the surface.
2. The *outer Helmholtz plane* with potential Ψ_d, consisting of a layer of bound, hydrated, and partially hydrated counterions.
3. The *diffuse layer*, composed of mobile co-ions and counterions, in which resides the slip plane bearing the ζ-potential.

In most cases, the outer Helmholtz plane and the slip plane are situated close to each other, allowing the approximation of Ψ_d with the ζ-potential for practical purposes.The slip plane, or shear surface, is an imaginary plane separating ions that are immobile at the surface from those that are mobile in solution. The ζ-potential at this plane can be experimentally determined, and is therefore an important parameter in colloid science for determining the stability of particles, and in μTAS for de scribing fluid flow in channels. The bulk liquid flow that occurs when the diffuse part of the EDL slips over a

charged surface in response to an applied electric field is the origin of all the double layer electrokinetic phenomena.

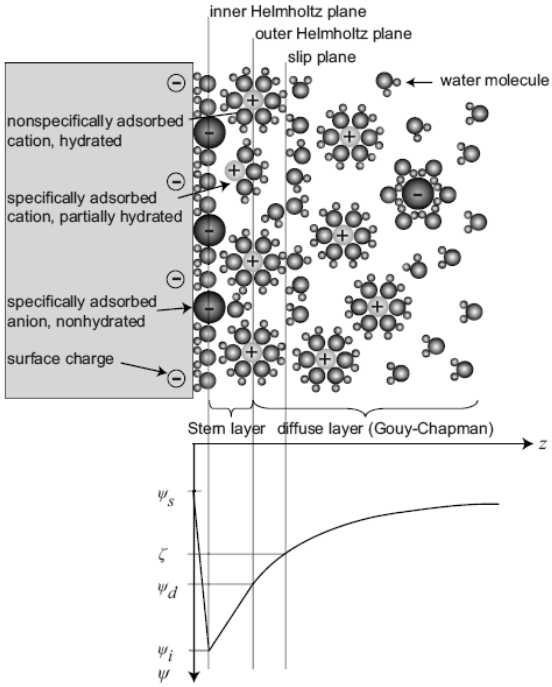

Figure 6.Electrical double layer.[34]

1.3.4 Electrokinetics

It studies the motion of electrically charged molecules and particles due to an applied electric field in a fluid (or vice versa). Electrokinetic phenomena are a family of several different effects that occur in heterogeneous fluids or in porous bodies filled with fluid. The term heterogeneous here means a fluid containing particles, which can be solid, liquid or gas bubbles with sizes on the scale of a micrometer or nanometre. This field covers for example (see Figure 7):

Electro-osmosis represents the liquid flow over a stationary charged surface that is due to a applied electric field.

Electrophoresis is the motion of a particle through a stationary medium under the application of an external electric field. Note that particles could be ions or polar molecules.

Streaming potential is the potential difference at zero current that appears by applying an pressure gradient in order to drive a solution over a stationary charged surface (membrane, plug or capillary).

Sedimentation potential, Generation of a potential difference at zero current and hence an electric field by applying an external force, gravitational or centrifugal, to drive

particle motion trough a stationary liquid matrix between two different electrodes at different positions. It is also known as the Dorn effect.

The first process is emphasized and subsequently its basic physics are presented. In electroosmosis, if the surface is negatively charged, the net excess of positive ions in the EDL will draw the liquid along because of viscous interactions, which results in flow toward the cathode. At the slip plane, the liquid velocity is zero and increases to a maximum value with the electro-osmotic velocity, at some distance from the wall, after which it remains constant at high ionic strength of the solution in a nanochannel.

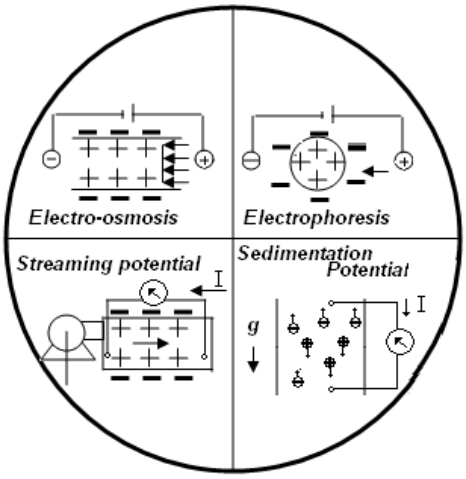

Figure 7.Electrokinetic phenomenon.

Measurements of tangential streaming potential and/or streaming current are commonly acknowledged as a convenient tool for the characterization of surface-charge properties of macroscopic surfaces, in particular, various membranes.

The conventional arrangement is that of two flat macroscopic surfaces put in parallel to form a relatively narrow channel. A dilute electrolyte solution is pumped along the channel, and the electric-potential difference or electric current is measured with a pair of reversible electrodes located close to the channel edges. Usually, the channel heights are by several orders of magnitude larger than the typical thickness of diffuse parts of electric double layers (EDL). Due to this, the surface conductance caused by the excess counter ion concentrations in the diffuse parts of EDLs can be neglected.

1.4 Taylor dispersion.

This phenomenon is explained in Figure 8. Imagine an infinitesimally thin tracer stripe in a circular channel of radius *w (a)*. Under a pressure-driven flow with velocity U_0, the stripe is convectively stretched into a parabolic shape whose width ΔW increases linearly with time (b). After a characteristic time scale $T_{D=}w^2/D$, where *D* is diffusion, for tracers to diffuse across the channel, the parabola is “smoothed” into a plug of width

$W_{TD}=U_0w^2/D$ (c). The plug can be broken into many thin stripes, each of which subsequently undergoes processes (a)–(c) to be smoothed into plugs of width W_{TD} on a time scale T_D. A tracer thus takes a random step of size equal or $<W_{TD}$ on each time step T_D, causing the stripe to evolve as a Gaussian spreading with effective diffusivity $D_{eff}\sim U_0^2w^2/D$.

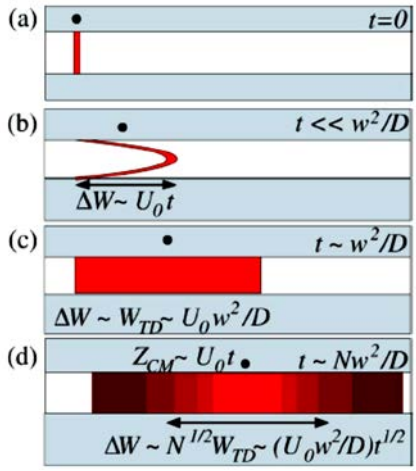

Figure 8. Schematic view of Taylor dispertion.[40]

1.4.1 Modelling of Taylor-Aris hydrodynamic dispersion for micro-/nano-channels

In micro-/nano-fluidic systems, the phenomenon of concentration polarization has already been observed experimentally in several distinct ways. Typically, the theoretical models have been based on the coupled Nernst-Planck, and Poisson equations (the latter sometimes replaced by the condition of local electric neutrality). Attempts have also been made to take into account the electro-osmosis [13, 41]. However, only the net electroosmotic flow was accounted for, whereas the electroosmotic circulation and the corresponding hydrodynamic dispersion, was disregarded.

On the other hand, compared to the “classical” configurations, at current densities typical for the electrically-driven micro-fluidics, micro-channels usually exhibit strong electroosmotic flows. In the previous theoretical studies, these flows have not been explicitly considered in full on the grounds that the electroosmotic permeability of serial connections of nano- and micro-fluidic systems is controlled by their nano-fluidic components (due to the much higher hydraulic resistance of the latter).

Here, the electroosmotic permeability is known to be reduced due to the overlap of diffuse parts of double electric layers [42] and the local electric-field strength is also reduced due to the surface conductance. This reasoning is basically correct but relates

only to the electroosmotic flows averaged over the cross-section of micro-channels. Actually, the situation is somewhat more complicated.

In a micro-channel “plugged” by a component with much higher hydraulic resistance and lower electroosmotic permeability (for example, a battery of parallel nano-channels), there is a gradient of hydrostatic pressure that drives the fluid in the direction opposite to the electro-osmosis so that the net volume flow turns out equal to the reduced flow through the “nano-block”. However, the velocity profiles of electroosmotic and pressure-driven flows are quite different. The electroosmotic profile is “plug-like” (in sufficiently broad micro-channels) whereas the profile of pressure-driven flow is parabolic. As a result of superposition (and almost complete compensation) of these two flows, the fluid close to the microchannel walls flows in the direction of electro-osmosis (and the local fluid velocity here corresponds to the normal rates of electro-osmosis in micro-channels) whereas close to the middle of the micro-channel the flow occurs in the opposite direction, see Figure 9. This phenomenon is referred to as electroosmotic circulation (EOC) and is important, for example, in the context of optical measurements of micro-electrophoresis. Close to the micro-/nano-interface, this flow pattern takes the form of a system of two counter-rotating vortices “returning” the electroosmotic wall flow to the middle of the micro-channel as a pressure-driven backflow [43].

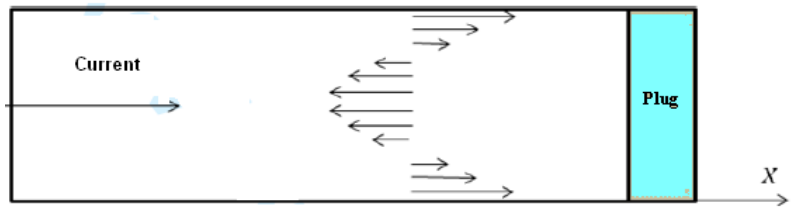

Figure 9. Schematic representation of the superposition of the velocity distribution of an electroosmotic and a pressure driven flow.

The rate of electro-osmosis is proportional to the electric field strength. At the micro-/nano interface where the buffer concentration goes down, the electric field strength strongly increases [44]. This causes a proportional increase in the local rate of electro-osmosis close to the channel walls. Due to the circulation flow pattern (arising because of the continuity of volume flow) this also means an increase in the rate of the pressure-driven backflow. The observed non-linear electro-osmosis has been qualitatively interpreted [45, 46] in terms of non-equilibrium space charge and the so-called electro-osmosis of the second kind (or induced-charge electroosmosis) predicted theoretically by Dukhin and Mishchuk [47].

In chemical engineering, it is well known that parabolic fluid velocity profiles give rise to the so-called hydrodynamic dispersion, which can be formally likened to an

increase in the solute diffusivity [48, 49]. The hydrodynamic dispersion is one of the principal sources of band broadening in liquid chromatography and it can also noticeably contribute to the band-broadening in capillary electrophoresis [50].

Using the Taylor-Aris concept of hydrodynamic dispersion [48, 49] for the description of dynamics of concentration-polarization phenomena close to nano-/micro-interfaces It can be shown that hydrodynamic dispersion leads to dramatic changes in the system behaviour, in particular, to the disappearance of limiting current phenomenon.

It is well known that mismatches in electrokinetic properties between micro- and nano-channels give rise to superposition of electroosmotic and pressure-driven flows in micro-channels. On the other hand, parabolic or similar flow profiles are known to give rise to the so-called hydrodynamic (Taylor-Aris) dispersion, which can be formally assimilated to an increase in the solute diffusivity. It is demonstrated theoretically that taking into account these phenomena modifies considerably the pattern of current-induced concentration polarization of nano-/micro-interfaces as compared to the classical model of unstirred boundary layer.

In particular, the hydrodynamic dispersion leads to disappearance of limiting current. It is also shown that at essentially “over-limiting” current densities, the time-dependent profiles of salt concentration in micro-channels behave like sharp concentration “fronts” moving away from the interface until they reach the reservoir end of micro-channel. Under galvanostatic conditions, these “fronts” move with practically constant speed directly proportional to the current density, Figure 10. The sharp transition from a low-concentration to a high-concentration zone can be useful for the analyte pre-concentration via stacking.

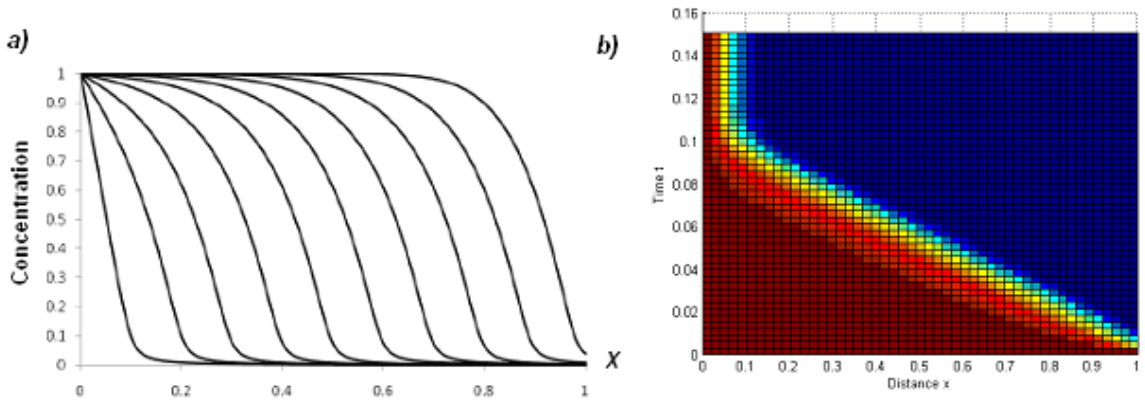

Figure 10.Time dependent profiles of salt concentration. a) Each curve represents a different distribution of the concentration in time, scaled with the initial condition. b) Propagating constant speed of the moving fronts; the red colour represents the initial condition and it can be seen how the diluted solution (blue) moves linearly respecting time.

On the other hand, it has been demonstrated that EOC could be a way to reduce the CP near porous media used in microfluidics systems which is related to the over-limiting current phenomenon [51, 52]. EOC enhances considerably the hydrodynamic dispersion and results in a specific distribution of solutes in micro-channels. The applicability of the Taylor-Aris Dispersion theory to the description of the mass transport in narrow and long channels under EOC have been subject of recent studies [52,53].

Yaroshchuk et al. [52] used a 1D approach to describe the distribution of an electrolyte in a microchannel with a micro-/nano-interface, in order to show that the hydrodynamic-dispersion mechanism becomes effective in much broader micro-channels. In turn, the surface-conductance mechanism is responsible for the appearance of deionization "shocks" in sub-micro-channels and in consequence those mechanisms operate under very different conditions. Therefore one of them can be disregarded when considering the other.

In contrast, Rubinstein and Zaltzman [53] showed the dependence of the distribution of a non-electrolyte with a constant buffer electrolyte inside a channel with different boundary conditions at the channel ends by solving the respective 2D convective-diffusion problem. To sum up, it is necessary to study the transport phenomena in microfluidics systems in order to understand the particularities of the concentration polarization, concentration shocks and other aspects such as hydrodynamic dispersion.

1.5 References

1. U. S. National Science and Technology Council Committee on technology subcommittee on nanoscale science, engineering and technology. Supplement to the President's Budget, May 2009. http://www.nano.gov. 13/04/14
2. H. J. Fecht and M. Werner, The Nano–Micro Interface. Bridging the Micro and Nano Worlds. Ed. Wiley-VCH, 2004.
3. U.S. National Science and Technology Council Committee on technology subcommittee on nanoscale science, engineering and technology. Strategic plan , Dec 2007. http://www.nano.gov. 13/04/14.
4. COM(2007) 505 final. Nanosciences and Nanotechnologies: An action plan for Europe 2005-2009. First Implementation Report 2005-2007. http://cordis.europa.eu/nanotechnology/actionplan.htm. 13/04/14.
5. D. N. Breslauer, P.J. Lee and L.P. Lee. "Microfluidics-based systems biology". Mol. BioSyst., 2, 97–112, 2006.
6. T. M. Squires and S. R. Quake, "Microfluidics: Fluid physics at the nanoliter scale", Reviews of Modern Physics, 77- 3, 2005.
7. J. de Jong, R. G. H. Lammertink and M. Wessling, "Membrane and microfluidics a review", Lab Chip, 6, 1125–1139, 2006.

8. J. C. T. Eijkel and A. van den Berg, “Nanofluidics: what is it and what can we expect from it?”, Microfluidics and Nanofluidics 1, 249-267, 2005.
9. A. Plecis, “Electropreconcentration with Charge-Selective Nanochannels”. Analytical Chemistry, 80, 9542–9550, 2008.
10. Z. Yuan, A. L. Garcia, G. P. Lopez, D. N. Petsev. “Electrokinetic transport and separations in fluidic nanochannels”. Electrophoresis. 28(4) 595-610, 2007.
11. T. A. Zangle, A. Mani, and J. G. Santiago, “Theory and experiments of concentration polarization and ion focusing at microchannel and nanochannel interfaces”, Chemical Society Reviews, 39, 1014-1035, 2010.
12. A. Plecis, R. B. Schoch, and P. Renaud, “Ionic Transport Phenomena in Nanofluidics Experimental and Theoretical Study of the EEE on a Chip”, Nano Letters 5-6, 1147-55, 2005
13. A. Mani, T.A. Zangle, J.G. Santiago, “On the Propagation of Concentration Polarization from Micro-Nanochannel Interfaces” Part II, Langmuir, 25, 3909-3916, 2009
14. A. Höltzel and U. Tallarek, “Ionic conductance of nanopores in microscale analysis systems: Where microfluidics meets nanofluidics”, Journal of Separation Science, 30, 1398–1419, 2007.
15. Leinweber and Tallarek, “Concentration Polarization based Nonlinear Electrokinetics in Porous Media”, Journal of Physical Chemistry, 109, 21481-21485, 2005.
16. Q. Pu, J. Yun, H. Temkin S. Liu, “Ion-Enrichment an Ion-Depletion effect of Nanochannel structures”, Nano Letters, 4, 1099-1103, 2004.
17. K. Scott, Handbook of Industrial Membranes, 2nd ed, Elsevier Advanced Technology: Oxford,UK, 1998.
18. C. Ronco and D. N. Cruz, “Hemodialysis, from basic research to clinical trials”, Ed. Karger , Basel, Switzerland. 2008
19. F. A. Morrison and J. F. Osterle, “Electrokinetic Energy Conversion in Ultrafine Capillaries”, Journal of Chemical Physics 43, 2111-2115, 1965.
20. H. Daiguji, P. Yang, A. J. Szeri, and A. Majumdar, “Electrochemomechanical Energy Conversion in Nanofluidic Channels”, Nano Letters 4, 2315-2321, 2004.
21. S. Liu, Q. Pu, L. Gao, C. Korzeniewski, and C. Matzke, “From nanochannel-induced proton conduction enhancement to a nanochannel-based fuel cell”, Nano Letters 5, 1389-1393, 2005.
22. T. S. Sorensen, Surface chemistry and electrochemistry of membranes; vol. 79, Marcel Dekker, Inc.: New York, USA, 1999.
23. R. D. Noble and S.A. Stern, “Membrane separations technology, Principles and Applications”, Membrance Science and Technology Series, 2, Elsevier Science B.V. 1995, Amsterdam, The Netherlands.
24. A. J. Burggraaf, “Fundamentals of inorganic membrane science and technology”, Membrane Science and Technology Series, 4, 1996, Amsterdam, The Netherlands.
25. T. Kuo, D. M. Cannon Jr, M. A. Shannon, P. W. Bohn, J. V. Sweedler, “Hybrid three-dimensional nano-microfluidic devices using molecular gates”, Sensors and Actuators A Physical 102, 223-233, 2003.

26. D. J. Harrison, K. Fluri, K. Seiler, Z. Fan, C. S. Effenhauser, and A. Manz, "Micromachining a Miniaturized Capillary Electrophoresis-Based Chemical Analysis System on a Chip," *Science* 261, 895-897, 1993.

27. T. Vilkner, D. Janasek, and A. Manz, "Micro total analysis systems. Recent developments," *Analytical Chemistry* 76, 3373-3385, 2004.

28. H. Andersson and A. van den Berg, "Microfluidic devices for cellomics: a review," *Sensors and Actuators B-Chemical* 92, 315-325, 2003.

29. F. Martin, R. Walczak, A. Boiarski, M. Cohen, T. West, C. Cosentino, and M. Ferrari, "Tailoring width of microfabricated nanochannels to solute size can be used to control diffusion kinetics", *Journal of Controlled Release* 102, 123-133, 2005.

30. F. J. Martin and C. Grove, "Microfabricated Drug Delivery Systems: Concepts to Improve Clinical Benefit", *Biomedical Microdevices* 3, 97-108, 2001.

31. F. Helfferich, Ion exchange, McGraw-Hill: New York, USA, 1962.

32. H. Strathmann, Ion-Exchange Membrane Separation Processes; vol. 9, Elsevier B.V.: Amsterdam, The Netherlands, 2004.

33. N. J. Petersen, D. Dutta, J. P. Alarie, and J. M. Ramsey, "Study of Interface Conductivity and its Possible Applications," 8th International Conference on Miniaturized Systems in Chemistry and Life Sciences, Micro Total Analysis Systems 2004, 348-350, Eds. T. Laurell, J. Nilsson, K.

34. I. Rubinstein, *Physical Electrochemistry*, Marcel Dekker, Inc.: New York, USA, 1995.

35. E. L. Cussler, Diffusion, Mass Transfer in Fluid Systems, 2nd ed, Cambridge University Press: New York, USA, 1997.

36. A. Yaroshchuk, O. Zhukova, M. Ulbricht, and V. Ribitsch, "Electrochemical and other transport properties of nanoporous track-etched membranes studied by the g current switch-off technique," Langmuir 21, 6872-6882, 2005.

37. G. T. A. Kovacs, "Introduction to the theory, design and modeling of thin-film microelectrodes for neural interfaces," in Enabling technologies for cultured neural networks, Eds. D. A. Stenger and T. M. McKenna, Academic Press, Inc.: San Diego, USA, 1994.

38. H. H. Girault, Analytical and Physical Electrochemistry, Marcel Dekker: Basel, CH, 2004.

39. Y. Oh, A. L. Garcia, D. N. Petsev, G. P. Lopez, S. R. J. Brueck, C. F. Ivoryc and S. M. Han, Effect of wall–molecule interactions on electrokinetic transport of charged molecules in nanofluidic channels during FET flow control, Lab Chip, 9, 1601–1608 2009.

40. T.M. Squires, S. R. Quake, Microfluidics: Fluid physics at the nanoliter scale, Reviews of Modern Physics, 77, 978-1007, 2005.

41. J. Han et al, "Amplified Electrokinetic Response by Concentration Polarization near Nanofluidic Channel", Langmuir 25, 7759–7765, 2009.

42. S. Pennathur andJ. G. Santiago. "Electrokinetic Transport in Nanochannels. 1. Theory". Analytical Chemistry 77 (21), 6772-6781, 2005

43. N. A. Mishchuk, F.Gonzalez-Caballero, "Nonstationary electroosmotic flow in closed cylindrical capillaries", Electrophoresis, 27, 661-671, 2006.

44. K. Huang., R. Yang, “A nanochannel-based concentrator utilizing the concentration polarization effect”, Electrophoresis, 29, 4862–4870, 2008.

45. S. J. Kim, L. D. Li, J. Han, “Amplified Electrokinetic response by concentration polarization near nanofluidic channel” Langmuir, 25, 7759–7765, 2009.

46. S. J. Kim, Y. C. Wang, J. H. Lee, H. Jang, H, J. Han, “Concentration polarization and nonlinear electrokinetic flow near a nanofluidic channel” Physical Review Letters, 99, 044501, 2007

47. S. S. Dukhin, N. A. Mishchuk, A. A. Tarovskii, “Electrophoresis of the 2nd Kind”, Colloid journal of the USSR, 49, 544-545, 1987.

48. G. Taylor,” Dispersion of soluble matter in solvent flowing slowly through a tube” Proc. Royal Soc. (London), 219A, 186-203, 1953.

49. R. Aris, “On the dispersion of a solute in a fluid flowing through a tube” Proc. Royal Soc. (London), 235A, 67-77, 1956.

50. E. Zholkovskij, J. Masliyah, “Hydrodynamic dispersion due to combined pressure-driven and electroosmotic flow through microchannels with a thin double layer”, Analytical Chemistry, 76, 2708-2718, 2004.

51. Dydek, E. Victoria, “Overlimiting Current in a Microchannel.” Physical Review Letters 107:118301, 2011

52. A. Yaroshchuk, E. Zholkovskiy, S. Pogodin, and V. Baulin, “Coupled concentration polarization and electroosmotic circulation near micro/nanointerfaces: taylor-aris model of hydrodynamic dispersion and limits of its applicability”, Langmuir 27:11710–11721, 2011

53. Rubinstein, I, and B Zaltzman. “Convective diffusive mixing in concentration polarization: from Taylor dispersion to surface convection.” Journal of Fluid Mechanics 728:239–278, 2013.

Objectives

Based in the introductory chapter, the objectives of this thesis are:

Evaluate the applicability of the Model of Taylor-Aris hydrodynamic dispersion in long and narrow microchannel for the description of coupled concentration-polarization and electroosmotic-circulation phenomena near micro-/nano-interfaces. It includes derive analytical expressions and use of numerical simulations to determine the applicability of the theory to the description of solute transport within a channel with a flow formed by oppositely directed electroosmotic and pressure driven flows for electrolyte and nonelectrolyte species.

Investigate numerically as well as experimentally streaming current measurements for characterization of porous media with commercially available electrokinetic analyser with an adjustable gap cell for mounting sample films with planar surface, in order to determine the influence of hydrodynamic effects under undeveloped flow conditions within a range of channel dimensions. Compare the differences between of nanoporous materials against coarser porous and nonporous substrates.

Develop numerical routines to study ion transport trough nanoporous media, taking in to account single or mixtures of different electrolytes, in order to explore the behaviour of the porous media under different applications at micro scale. Although they are important to understand the phenomena in miniaturized processes, can also be considered useful tools for interpreting results obtained at macro scale.

Evaluate the hollow fibre liquid-liquid membrane contactors (HFMC) as polishing step for removal of low levels of ammonium from water. Determine a model and validate it to describe the Influence of operational conditions such as flow rate, pH ammonium concentrations and buffer capacity of the system for both open and close loop configurations.

2.1 Motivation

The potential impact of the nano- and micro-technologies has been outlined in the previous chapter. Likewise, the problems related to the use of membranes in devices of such technologies have been reviewed. From here and after the purpose of this thesis is going to be outlined.

Just as in the macro scale, the phenomenon of concentration polarization is one of the main issues that must be addressed technologically in order to implement correctly the use of membranes at micro-scale. Accordingly, it is necessary to test the applicability of Taylor-Aris hydrodynamic dispersion theory for the description of coupled concentration-polarization and electroosmotic-circulation phenomena near micro-/nano interfaces with experimental and simulation work. A methodology to test such applicability and the subsequent results obtained from it are needed to understand the physics behind many micro-processes. Its study can be useful for the description of early stages of polarization in such systems and in turn, it can be used as a reference (applicable at some distances away from the nano-/micro body) with more sophisticated numerical models.

It is clear that there is a big interest in the development of new porous materials including its subsequent integration in biomedical devices and industrial applications. Consequently, the description of the particularities of the nanoporous media (for example membranes) and the development of characterization techniques are crucial to control the behaviour of systems which include separation and purification processes with such technologies.

The implementation of microfluidic technologies at industrial scale is one of the major challenges to face; nevertheless there are some devices which are already being used systematically at industrial level for separation purposes fulfilling the criteria of characteristic length needed for considering them inside the group of the microfluidic technologies. Such is the case of the hollow fibre membrane contactors where the evaluation of the mechanisms involved for the gas separation under the bases of microfluidic technologies can be useful to implement their fundamentals in the development of miniaturized versions of them that can be used in new bio-chemical applications.

2.2 Thesis outline

This thesis is divided in two parts, modelling and characterization applied at two scales, micro and macro. The first part of the thesis is devoted to the description of characteristic phenomena in microfluidic devices. In such section, the applicability of the Taylor and Aris dispersion theory for the description of the mass transport of electrolyte

and nonelectrolyte solutions inside a microchannel under electroosmotic circulation is evaluated. Next, an improvement is going to be developed in the characterization techniques of nanoporous media. The effect of hydrodynamic conditions is evaluated in the measurement of the zeta potential by monitoring the streaming current coefficient in condition of undeveloped flow.

The second part contains the work developed for the characterization of nanofiltration membranes in terms of their permeances, by defining a mathematical model capable of taking in to account electrolyte mixtures as working solutions. Finally the process of ammonia removal from water by hollow fiber membrane contactors is going to be toughly studied in the last part of the thesis.

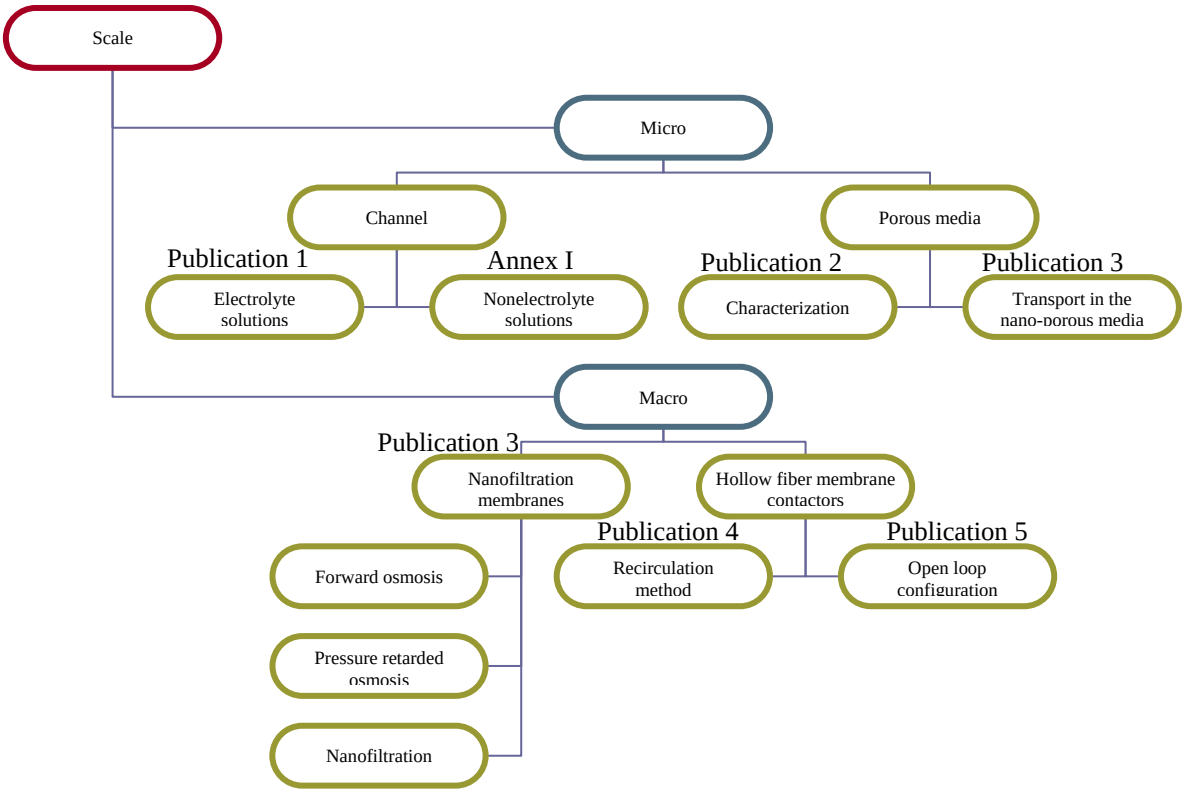

Figure 11.Scheme of the thesis outline.

This thesis is based in the next publications:

Publication 1 (P1):

E. E. Licon Bernal, V. I. Kovalchuk, E. K. Zholkovskiy, A. Yaroshchuk, Hydrodynamic dispersion in long micro-channels under conditions of electroosmotic circulation, I Non-electrolytes, Microfluidics and Nanofluidics, In press, (2014)

Publication 2 (P2):

Andriy Yaroshchuk, Edxon Eduardo Licón Bernal, Thomas Luxbacher, Electrokinetics in undeveloped flow, Journal of colloid and interface science, 410, 195–201, (2013)

Publication 3 (P3):

Andriy Yaroshchuk, Merlin L. Bruening and Edxon Eduardo Licon Bernal, Solution-Diffusion-Electro-Migration model and its use for analysis of Pressure-Retarded Osmosis and Forward Osmosis, Nanofiltration in multi-ionic solution, Journal of Membrane Science, 447, 463-476, (2013)

Publication 4 (P4):

E. Licon, S. Casas, A. Alcaraz, J.L. Cortina, C. Valderrama ,Ammonia removal from water by liquid-liquid membrane contactor under closed loop regime, proceedings from the European COMSOL Conference 2012

Publication 5 (P5):

Edxon Licon, Mònica Reig, Pilar Villanova, Cesar Valderrama, Oriol Gibert and José Luis Cortina, Ammonium removal by liquid-liquid membrane contactors in water purification process for hydrogen production, Desalination and Water Treatment, In press, (2014)

Results and discussion

On this chapter the main results are presented according to the objectives and the publications produced during the development of this thesis. The reader is encouraged to check the publications in order to know the methodology in each case.

3.1 Hydrodynamic dispersion in long micro-channels under conditions of electroosmotic circulation (P1 and Annex 1)

A parametric study has been done to evaluate the applicability of the Taylor dispersion theory by means of a ratio of the flux calculated numerically and the obtained analytically (R) in the case of different non-electrolyte concentrations at the edges of an open microchannel channel (P1).

The ratio R was calculated for different values of aspect ratio (λ) and Peclet number (Pe) by varying the length of the channel (L) and the concentration of the buffer electrolyte (cb) and the results are shown in P1-Figure 11. It is seen that as a larger deviation values of around 15 % are obtained.

For the system with different concentration of electrolyte at the edges of the microchannel, the Taylor-Aris approach is valid as a first-order approximation only, because the contribution of the transversal convection leads to deviations from the behavior expected according to this approach. To evaluate the applicability of the Taylor-Aris approximation a certain quantitative criterion is needed. As such criterion, it can be considered here the deviation from unity of the ratio of the actual solute flux, calculated numerically, to that given by the Taylor-Aris approximation (see Annex1-Eq. 9).

Deviation of the numerically calculated parameter R from unity can be a useful criterion to identify the particular conditions and regions of the channel, for which the transport phenomena can be interpreted in terms of TAD mechanism. In Annex 1-Figure A9, the profiles of the parameter R are presented for a channel of 4 mm length and 100 μm half-height. The effect of the current density is evaluated for a concentration ratio of 10 for two directions of electroosmotic velocity: Annex 1-Figure A9a shows the case where the electroosmosis is directed from x = 0 to x = L, whereas Figure A9b corresponds to oppositely directed electroosmotic flow. Both cases show small deviations from the TAD theory in the inner part of the channel and strongly increasing deviations in the small regions near to the channel ends. Furthermore at relatively low current densities, the deviations from TAD analysis are lower and they are increasing with the current. Moreover, by comparing the two graphs a clear dependence on the current direction is

evident. Although they look as to have a mirror-like symmetry, the deviation is larger for the case of Annex1-Figure A9a.

In P1-Figure 2 longitudinal profiles of normalized average concentration are presented for various Péclet numbers. There are three characteristic zones: the inner part where there is a clear linear dependence on the coordinate, and the two “jumps” at the edges. The “jumps” get stronger with increasing Péclet number, which results in a decrease in the slope of the linear part. The linear dependence in the middle corresponds to the solute transfer with a constant dispersion coefficient that follows from P1-Eq.(13) for steady-state conditions. This is an indication that the Taylor-Aris approach is valid for this part of the channel. In the boundary layers near the channel ends (P1-Figure 1-b and 1-c), hydrodynamic dispersion appears not sufficient to provide continuity of the solute flux in these regions.

The profiles of local concentration at various longitudinal cross-sections show a more complicated behaviour as compared to the average concentration (P1-Figure 3). The longitudinal profiles of local concentration are also linear within the inner part of the channel, reflecting the Taylor-Aris behaviour. However, there are transition zones near the channel edges whose length strongly depends on the transversal coordinate, y. This length is very small in those parts of the entrance cross-sections, where the solution leaves the channel (close to the middle horizontal plane, $y \approx 0$, at the left- and close to the walls, $y \approx \pm h$, at the right-hand side), and it is much larger at the locations, where the solution enters the channel. Moreover, for the inflowing conditions the longitudinal concentration gradient is smaller than in the inner part of the channel, whereas for the out-flowing solutions it is larger (P1-Figure 3c). For intermediate planes (at $y = 4h/5$, for example) the longitudinal concentration gradient initially increases with the distance, passes through a maximum and then approaches the constant value occurring in the inner part, but from above.

The size of transition zones where the Taylor-Aris behaviour does not occur strongly depends on the Péclet number, and the effect of Pe depends on the local flow direction. For the out-flowing solution (near the mid-plane at the “dilute” side and near the walls at the “concentrated” side) the transition zone gets shorter with increasing Pe, whereas for the inflowing solution it gets longer. This is seen from the shape of contour graphs shown in P1-Figure 4, represented by the fixed-concentration lines corresponding to the local concentrations at the edges of the transition zone, $x = xs$, on the walls, $y \approx \pm h$, for various Pe. The size of the transition zones and the concentrations at their edges are listed in P1-Table 1. The method used to determine the size of the entrance zones, xs, and the concentrations at the edges is discussed in P1.

In order to compare these two systems (electrolyte and not electrolyte), longitudinal cross-section profiles along the channel for three different heights are plotted for the electrolyte case in Annex1-Figure A4. Different slopes for these three cases are observed, what is explained by the difference in local conductivities. In contrast, for the system with transfer of non-electrolytes the profiles were running parallel for the same longitudinal cross-sections due to the constant buffer electrolyte concentration and constant conductivity in the channel. Since intensity of convection is dependent on the electric field, the boundary zone near the channel edge with more diluted solution (x = 0) is more pronounced than that on the opposite side. Additionally, as in the case of non-electrolytes, the length of this zone strongly varies with the transversal coordinate, y. The boundary zone is very small in those parts of the cross-section where the solutions leave the channel (at the side with diluted solution for $u_{eo} > 0$ this is near the middle horizontal plane, $y \approx 0$, and at the opposite side - near the walls, $y \approx \pm h$), and it is much larger at the locations, where the solutions enter the channel ($y \approx \pm h$ at the side with diluted solution and $y \approx 0$ at the opposite side).

Figure A5 is a contour plot of the reciprocal concentration. It shows the evolution of the profiles shape from the constant concentrations at the edges to the Taylor-Aris type profiles in the inner part of the channel. This profile type is defined by the concentration deviation within the inner part of the channel, given by P1-Eq. (17).

On the channel side with more diluted electrolyte concentration (close to x = 0 on this example) in vicinity of the walls, there are extended zones where the concentration almost does not change, remaining practically the same as at the edge. These zones arise due to protrusions of the external solution near the walls. The similar protrusion zone appears also on the right side of the channel (x = L), but in vicinity of the middle plane ($y \approx 0$). Such protrusions of the external solutions result in distortions of the transversal concentration profiles compared to those established within the inner parts of the channel away from its ends. At the internal edges of these region (x = xs and x = 1-xm) the concentration profiles transform gradually to the profiles corresponding to the TAD theory, P1-Eq. (17). The same effects within the entrance zones of the channel were observed also in the case of non-electrolytes transfer, considered in P1.

3.2 Correct interpretation of results of tangential electrokinetic measurements under undeveloped flows (P2)

In this section of the results, the electrokinetic phenomena in undeveloped flows are numerically and experimentally investigated. P2-Figure 8 shows the results of statistical treatment of a series of six repeated measurements carried out at the same

channel height. The data have been corrected for the streaming-current of asymmetry and mirror-reflected the data obtained for the negative pressure differences. In agreement with the simulation data from P2-Figure 6, the pressure dependence of streaming current is slightly sub-linear. The data obtained for the other channel heights were statistically treated in the same way and used to obtain the streaming-current coefficients (the factor by the linear term in the quadratic approximation) shown in P2-Figure 9. On the other hand, the results of numerical simulations were used to fit the channel-height dependences of these coefficients. In fitting this (in case of membranes), a nonzero streaming-current component was allowed to occur at zero channel height, in order to take into account the possible contribution of porous membrane supports.

In addition to the streaming current and potential, The SurPASS instrument (see methodology on P2) measures online the channel electrical conductance and the solution electric conductivity. These quantities can be combined in this way to obtain an alternative estimate of channel height (P2-Eq. 12).

P2-Figure 10 shows the “conductance” channel height plotted vs. the “hydrodynamic” height calculated from the hydraulic permeability by taking into account the undeveloped flow pattern.

P2-Figure 10b additionally confirms the correctness of our estimates of channel height via numerical simulations of undeveloped flow. Indeed, in case of nonporous substrate, the extension of linear trend line to zero “hydrodynamic” channel height passes almost exactly through zero. For nonporous substrates, the conductance can occur only through the channel. Since the electrical conductance is unaffected by the flow hydrodynamics, one can consider the channel heights estimated from the electrical conductance as reference values, in this case. The fact that they practically coincide with the “hydrodynamic” values corroborates the correctness of our CFD simulations. At the same time, P2-Figure 10a shows that when the “hydrodynamic” channel height is estimated in the conventional way (by using Hagen–Poiseuille equation), the extension of linear trend line does not pass through the origin, and the (negative) offset is quite noticeable.

For the membranes, there are nonzero intersects of extensions of linear trend lines to zero channel height. This is indicative of some conductance through the porous substrates. This phenomenon is much more pronounced for the MF membrane than for the NF membrane. This is not directly related to the fact that the MF membrane is “loose” while the NF membrane is denser. The “denseness” of NF membrane is concentrated in a vanishingly thin barrier layer that does not make any appreciable contribution to the

electrical conductance along the membrane. This phenomenon is controlled by the porous poly-sulfone and nonwoven polyester sub-layers. According to P2-Table 1, the conductivity of parallel connection of these materials is on average 20 times lower than the conductivity of equilibrium electrolyte solution. Although the mechanism of this relatively low conductivity is not quite clear, it can be noted that this observation correlates with the fact that commercial NF/RO membranes have revealed themselves as poor performers in the processes of Pressure-Retarded Osmosis and Forward Osmosis. This has been attributed to the severe internal concentration polarization, which in turn is due to a low diffusion permeability of membrane support layers. For relatively coarse-porous materials like those supports the diffusion permeability and electric conductivity can be expected to be roughly proportional. It was suggested that the low diffusion permeability of those materials could be due to their poor wettability because of partial hydrophobicity.

It is confirm then that the aforementioned sub-linearity occurs for nonporous as well as porous substrates. It is also demonstrate that the channel heights estimated from the volume flow rate by using numerical simulations of undeveloped flows are in very good agreement with the reference values obtained from the electrical conductance (in contrast to the values estimated by using the conventional approach of Hagen–Poiseuille equation). The numerical fitting of channel-height dependences of streaming-current coefficient enables us to separate the contributions of external surface and porous sub-structure (in case of porous substrates) and obtain quite reasonable values of (effective) zeta-potentials in both cases. Nonetheless, the accuracy of experimental data deteriorates with increasing channel height, so it is generally advisable to vary the heights within a range below 100–150 microns.

3.3 Modelling of the transport of electrolyte mixtures trough nanoporous layers (P3)

This section presents an analytical solution to the differential equations that govern the electrically coupled transport of multi-electrolyte solutions through a barrier layer (membrane) in which the Solution-Diffusion-Electro-Migration model applies. This model disregards convective coupling between the trans-membrane flows of ions and solvent and uses composition-independent single-ion permeabilities to quantify ion transfer through the membrane

P3-Figure 3 shows calculated (using P3-Eq. 47) reciprocal transmissions (1/(1-rejection)) of nanofiltration of ternary electrolyte mixtures of arbitrary composition of a (+1:+2:-1) electrolyte mixture through a membrane whose ion permeabilities mimic those

of a recently reported polyelectrolyte multi-layer membrane. P3-Figure 1 schematically depicts the separation.

The "rapid" single-charge cation, Na^+ (P3-Figure 3a), experiences negative rejections (reciprocal transmissions smaller than one) at small to moderate trans-membrane volume flows even when its feed mole fraction is as high as 0.6. This agrees with experimental data on the negative rejections of Na^+ from $MgCl_2$/NaCl mixtures at approximately one-to-one feed composition. Addition of the "rapid" cation to the feed makes the rejection of the "slow" cation higher (reciprocal transmission increases, P3-Figure 3b) since electromigration decreases because of the higher membrane conductance resulting from more of the "rapid" cation. The rejection of the common anion strongly depends on the feed composition (P3-Figure 3c) since it has to match the rejections of either of the two cations in the two limiting cases of single salts. Notably, even low feed mole fractions of the "rapid" cation (14%) still decreases the rejection (and the reciprocal transmission) of the common anion. This occurs because the "rapid" cation has a disproportionally high impact on the membrane conductivity.

P3-Figure 4 illustrates the use of P3-Eq.53 for describing pressure-driven transport of trace ions added to a dominant ternary electrolyte. The membrane ionic permeabilities employed in these calculations are qualitatively similar to those of NF270 (Dow Chemical) membranes and decrease in the order $Na^+ > Cl^- > Mg^{2+} > SO_4^{2-}$. When $MgCl_2$ is the dominant salt in the feed solution, a spontaneously-arising electric field accelerates trace Na^+ transport (as well as Mg^{2+} transport), whereas when the feed solution contains mostly $MgSO_4$, the electric field retards Na^+ transport and accelerates SO_4^{2-}. The experimental rejections of trace Na+ were strongly negative (up to -100%) in $MgCl_2$ and positive and quite high (up to 90%) in $MgSO_4$. P3-Figure 4 shows the gradual transition from one of those two limiting cases to the other as the dominant feed composition varies. Generally, the contrast between the two limiting compositions increases with the trans-membrane volume flux. Nevertheless, at the highest flux, the negative rejections start to decline. This corresponds to fluxes to the right from the minimum seen in P3-Figure 3a. The cross-over from the negative rejections to the positive ones occurs at relatively large feed mole fractions of sulfates, which generally increase with the growing trans-membrane volume flow.

P3-Figure 4b also shows the rejection of Cl^- as a function of feed composition. With an increasing fraction of $MgSO_4$ in the feed, Cl^- rejection decreases and ultimately turns negative when the chloride essentially becomes a trace ion in the dominant $MgSO_4$. These negative rejections compare with the strongly positive rejections of sodium at the

same feed compositions. Comparable behavior would occur for a similar anion (for example, bromide) present as a trace. Thus, P3-Figure 4 clearly demonstrates that the rejections of cations and anions of a trace salt are very different and show opposite trends in rejections as functions of dominant-ion composition.

In Pressure-Retarded Osmosis (PRO), energy is harvested from the difference in salinities between a more concentrated (e.g., seawater) and a much less concentrated (e.g., river water) solution. Usually, the membrane is oriented with the barrier layer towards the more concentrated solution. For the sake of simplicity, in the sample calculations below, we shall assume the lower salinity to be zero.

Due to the higher hydraulic permeability (as compared to the barrier layers of RO-like membranes) the use of membranes with NF-like barrier layers could be beneficial in PRO configurations. However, low solute permeability is important to maintain osmotic pressure, and NF membranes (commercial as well as laboratory-made PEML) have high permeabilities to single-charge cations and anions. Nevertheless, commercial NF membranes have low permeabilities to sulfates. Some PEML membranes have very low permeability to magnesium ions. Both SO_4^{2-} and Mg^{2+} are present in small but significant amounts in seawater or concentrated seawater brines, the most probable draw solutions for PRO. Thus, we considered whether the osmolality due to those ions would be sufficient to give significant osmotic flows and what effect more abundant “rapid” ions like sodium and chloride would have on these flows.

P3-Figure 5 shows the calculated dependences of trans-membrane volume flow on the relative concentration of NaCl added to the draw solution initially containing either Na_2SO_4 (barrier layer similar to a commercial NF membrane) or $MgCl_2$ (supported PEML-like barrier layer).

The S parameter (structural parameter, viz. effective thickness of the support layer) in both cases is 380 μm, and the barrier-layer permeabilities are the same as used previously for these two examples. Notably, the permeability to Mg^{2+} is assumed to be higher than estimated from diffusion dialysis.

Notably, the volume flows under the conditions of just single low-permeability salts present in the draw solution are quite high compared to commercially-available FO membranes. This is in agreement with the experimental data reported for supported PEML membranes. However, counter intuitively, despite an increase in the draw-solution osmolality the addition of NaCl gives rise to initial decreases of osmotic flow with both types of membranes. This phenomenon occurs because of the electric field that

spontaneously arises due to the assumed very different permeabilities of the membrane barrier layer to SO_4^{2-} and Na^+ ("commercial" NF membrane) or to Mg^{2+} and Cl^- (PEML-like membrane). This electric field retards the "rapid" single-charge cations/anions but simultaneously accelerates their "rapid" oppositely-charged counterparts. As a result, the concentration of the rapid ions at the barrier-layer/support interface is higher than in the draw solution (this resembles the negative rejections of these ions in NF; see P3-Figure6). At small to moderate concentrations of added NaCl in the draw solution, the increase in the total ion concentration at the support/barrier-layer interface (due to the increase in the Cl^- or Na^+ concentrations) is larger than the increase in the total ion concentration in the draw solution. This leads to decreased trans-membrane volume flows. Further addition of NaCl to the draw solution makes the concentration increases at the support/barrier-layer interface relatively weaker (see P3-Figure 7), and the total ion concentration difference across the barrier layer starts to increase, which leads to the ultimate increase in the osmotic flow in P3-Figure 5.

Despite the initial decrease in the osmotic flow, its magnitude remains quite high even around the minima. It points to an interesting opportunity for driving osmotic processes by only some of the solutes (those which the membrane has low permeabilities to) in multi-ion solutions like seawater.

In Forward Osmosis, a semi-permeable membrane separates a highly concentrated draw solution from a less concentrated feed solution. In all practical applications, the ionic compositions of draw and feed solutions are different. Therefore, in this application one always deals with electrolyte mixtures. However, Forward Osmosis in multi-ionic solutions has not been addressed theoretically. Hancock et al. derived local relationships for the coupling of ion flows via spontaneously-arising electric fields. However, they did not solve the resulting differential equations. Here again we want to illustrate the opportunities offered by relatively loose NF-like membranes that have low permeabilities only to multiple-charge ions.

Due to its high solubility and osmolality $MgCl_2$ frequently serves as a draw solute in Forward Osmosis, especially with NF-like barrier layers. Consider an idealized configuration where a composite membrane separates a concentrated $MgCl_2$ draw solution and a lower-concentration NaCl feed solution. The membrane barrier layer faces the lower-concentration feed (the so-called FO configuration). P3-Figure 8 schematically shows the ion flows in the barrier layer.

When $MgCl_2$ diffuses through the barrier layer, the spontaneously-arising electric field retards the "rapid" chloride ions to make their diffusion stoichiometric to the "slow"

magnesium ions. This same field transports the sodium ions towards the feed solution to increase rejection. The calculated rejections in P3-Figure 9 demonstrate that this field can significantly reduce the trans-membrane flux of Na^+ to improve its rejection in the FO process as compared to a hypothetical pressure-driven process with the same membrane and the same trans-membrane volume flows.

3.4 Modelling and characterization of liquid-liquid membrane contactors (P4 and P5)

According to Figure 4, the ammonium Ammonia separation from water by a membrane contactor was simulated on transient state and compared with experimental data. Aqueous low concentrated solution of ammonium with high pH has been pumped inside a hydrophobic hollow fiber (lumen), sulfuric acid solution in the outside part. Two configurations were studied, on one hand the feeding solutions were in closed loop configuration and on the other hand an open loop configuration was used. In order to simulate the separation process, the model equations were developed considering radial-axial diffusion and convection in the lumen with a well-developed parabolic velocity profile.

In the P4-Figure 5 is shown how the concentration is decreasing when the fluid pass the lumen of a fiber, at the membrane surface the transport of the ammonia trough the membrane to the acid solution is occurring. Different simulations have been done. From the P4-Figure 6 is evident that this model is independent of the initial concentration set in the tank with ammonium chloride. According to P4-Figure 7 and P4-Figure 8, the improvement in the efficiency of this separation process by rising the pH or the flow rate is limited by some extend and this information can be used to optimize resources and energy needed to carry out the removal process.

In the case of the recirculation method, some experiments were done to validate of the mathematical model. In P4-Figure 6 is shown the evolution of the feeding tank concentration under different experimental conditions in terms of flow rate and initial pH. In the experiment 2 a poor removal of NH_4^+ was obtained because no buffer solution was added and pH was not constant. Next experiments were made with a buffered solution. The experiment 1 and 4 were performed under same conditions but the solutions were prepared on tap water and distillate water, respectively. Some deviation was observed in tap water experiment, but nevertheless, a good agreement is observed between experimental and simulated values.

For both cases ammonia removal was clearly affected by the solution pH. The equilibrium between the ammonia gas and ammonium ions depends on the solution's pH, making it the driving force responsible for the separation process.

Considering the open loop configuration case, On P5-Figure 4, it can be seen within the pH range studied, that the model fits the experimental data better at low pH than to at higher. Although the model does not consider the concentration of ammonia at the shell side, it was not comparable to the acid concentration. Even in hypothetical cases of comparable concentrations, it has to be taken into account that the parameter that controls the driven force is the ammonia partial pressure difference between both sides of the membrane. In order to have effects on this force, a substantial increase in the pH of the extracting solution must occur to move the ammonium equilibrium to ammonia gas, which was not the case for none of experiments carried out. Likewise, the trend predicted by the model follows qualitatively the tendency of the experimental data and moreover, a turning point is identified, which coincides with the pKa (pH = 9.3) and is the reaction equilibrium between ammonium and ammonia. Two different zones are also differentiated in the plot: one for pH values below the pKa where low values of removal are obtained. The predominant species is the ammonium and the presence of ammonia is low. The ammonia is the species that crosses the pores of the membrane and reacts with sulfuric acid resulting in ammonium sulfate, the minor presence of this species gives rise lower elimination rates. On the other hand, at pH values above the pKa higher removal efficiencies are obtained due to the dominant presence of ammonia gas and therefore, a greater number of molecules of the gas cross the membrane to react with sulfuric acid resulting in a higher removal performance. A further increase in the pH (> 10) not represent a significant increase in ammonia removal, that should be taken into account when designing the real operational conditions in order to save reagents consumption.

P5-Figure 5 shows the results of the experimental data and for removal of ammonium at different initial concentrations of ammonium. It can be observed that the trend of the evolution is similar for the six experiments. Nonetheless, when comparing against the profile obtained numerically differences between them are observed. As can be seen, this error does not have a clear dependence and make think that can be related to errors inherent to the experimental determinations. Accordingly, it can be considered that the removal of ammonium is independent of the initial concentration of the solution to be treated. This is in agreement with the result presented for several authors working in liquid-liquid mode but closed loop regime.

The other important parameter to be taken into account is the flow rate which affects the residence time of the solution inside the LLMC; the larger the flow rates the lower the efficiency of the contactor (see P5-Figure 6). For each experiment, its respective linear velocity (U) was calculated by means of P5-Eq. 15 and the results are presented as function of the reciprocal velocity (1/U).

According to P5-Figure 6, the model is substantially consistent with the experimental data. However, the fact that both are not identical can be attributed again to experimental error, such as the presence of any air bubbles in the circuit, the error in the ammonia selective electrode, among others. It can be seen, that at low values f of 1/U (at high flows) lower removal is reached. Additionally it can be seen that the profile presents a zones in which a small change in flow results in a large variation in ammonia removal. Nevertheless, it has to be taken in to account that very low flow rates may produce an extra resistance in the liquid phase.

From P5-Eq. 4 the overall mass transport coefficient can be calculated for each flow defined in the experimental part (P5-Table 1). P5-Figure 7 shows how this coefficient is almost independent to Reynolds numbers (in the lumen) larger than 6. Nevertheless the variation in the complete range is just about 1.5%. Calculated values of various parameters from the model equations are given in Table 4. In all the experiments, the flow can be consider laminar at both sides of the membrane due to the low values for their respective Reynolds numbers obtained with equation 12 (Table 1).

Taking into account all the results, it can be said that when the pH values promote a high concentration of ammonia and the flow rate maintain an adequate residence time, the LLMC will remove the same percentage of the ammonium from the feeding solution when working in open loop configuration irrespective of the feed concentration.

For instance, a constant fraction of the inlet ammonia concentration can be removed with a LLMC unit, this fraction obtained from experiments with pH of10 and flow rate of feed of 3.48x10-6 m3•s-1 was nearly 0.3. Figure 8 shows the ammonia concentration against number of modules (Nm) in series and it is observed that removal efficiency can by larger to 95% with three units.

Conclusions

In the description of the hydrodynamic dispersion in microchannels is important to point out that:

The applicability of the Taylor and Aris dispersion theory (TAD) under conditions of electroosmotic circulation in long straight channels connecting two reservoirs with different concentrations of a non-electrolyte and constant electrolyte concentration has been shown to be local in the inner part of the channel.

Under steady-state conditions, the concentration profile in the channel is a result of a balance of transversal diffusion and lateral convection. As the concentration profile is the same for all channel cross sections, the dispersion coefficient remains constant along the channel. This results in linear concentration profiles along the inner part of the channel.

In the boundary layers near the channel edges, which were called entrance zones, the concentration profiles are not fully developed because the boundary conditions require constant concentrations at the ends, which do not agree with the requirements of Taylor and Aris model. The entrance zones sizes are controlled by the Péclet number (Pe) and the height of the channel. These zones control the inner concentration gradient. With increasing Pe, the solutions from the reservoirs penetrate deeper into the channel, producing more noticeable deviations from the TAD approximation. It has been demonstrated that the dependence on Pe of the concentration inner gradient can be expressed in terms of only four dimensionless parameters ($\alpha_{1,2}$ and $\beta_{1,2}$) that can be determined numerically.

The results of numerical simulations show that when two different concentrations of electrolyte are used at the channel ends, its distribution within a major part of a long microchannel under conditions of electroosmotic circulation are in a good agreement with that predicted by the TAD formalism with the exception of only two boundary layers formed at the edges, as in the case of non-electrolytes. In this particular case the electroosmotic flow velocity is varying along the channel and the dispersion coefficient is not a constant but is a function of the local Pe. An approximate parametric description was proposed and it simplifies the calculations of the concentration distribution within the channel and the current-voltage characteristics of the system, which can be important for practical use in analysis of experimental data on electroosmotic circulation and concentration polarization in long micro-channels.

For tangential electrokinetic measurements using equipment which include variation in the channel height it is important to take in to account that:

According to both, experiments and numerical simulation, a nonlinear dependence of streaming-current coefficient on the channel height has been identified for typical equipment for tangential electrokinetic measurements with macroscopic surfaces as result of the undeveloped turbulent flow within a major part of the channel length with heights larger than 150 microns.

If the measurements are carried out at larger channel heights only and the data are linearly extrapolated to zero channel heights, the nonlinear dependence on the channel height can be mistaken for a contribution of porous sub-structure to the streaming current.

This study demonstrates that, in principle, accounting for the undeveloped flow pattern allows to single out the contribution of porous sub-structure to the streaming current even for larger channel heights.

This work presents an analytical solution to the differential equations required to describe simultaneous transport of electrolyte mixtures in barrier layers.

Such a model is important for understanding phenomena such as negative rejection and osmosis rates as a function of ion concentrations in feed and permeate solutions.

The model provides reasonable negative rejection values during nanofiltration of ions whose permeances differ greatly, e.g. Na^+ and Mg^{2+} or Cl^- and SO_4^{2-}. It also gives interesting trends in osmosis as a function of the draw solution concentrations, showing that addition of NaCl to a $MgCl_2$ draw solution initially decreases the volume flux.

The used examples demonstrate that spontaneously arising electric fields dramatically alter transport. Perhaps more importantly, calculations demonstrate that spontaneously arising electric fields may yield much higher NaCl rejection in forward osmosis than reverse osmosis when using highly permeable nanofiltration membranes.

The development of an analytical model for coupled transport of 3 ion classes, and a single non-linear ordinary differential equation for ions with 4 ion classes permits rapid calculations, which in turn, enable to understand the transport of complex electrolyte mixtures in osmotic processes.

For instance, t*he use of a Liquid-Liquid Membrane Contactor (LLMC) to improve the water quality by removing traces of ammonium*

The mathematical model here presented has been validated experimentally under several conditions. It can be used to evaluate the LLMC performance for ammonia removal from aqueous solutions under different processing conditions and to define the operational parameters necessary to remove ammonia efficiently.

The most important parameters to control during the experiment are the flow rate and the pH, mainly the last one, due to the high dependence in the chemical equilibrium of ammonium conversion to ammonia.

In view of the results of this study, the technology of LLMC operating in open-loop configuration is potentially suitable to remove water with low levels of ammonium. A simple expression was determined to estimate the number of membrane modules placed in series necessary to reach a given target value. The maximum efficiency observed experimentally for single step was a removal of around 78% under feed values of pH, initial concentration, and flow rate of 10, 2.72 × 10−6 $m^3 \cdot s^{-1}$ and 15 $mg \cdot L^{-1}$, respectively.

Annex 1

Hydrodynamic dispersion of electrolytes in long micro-channels under conditions of electroosmotic circulation

Introduction

Concentration Polarization (CP) is a fundamental phenomenon which can reveal itself in electrode systems or in microheterogeneous systems, such as semipermeable membranes, ion-exchange resins, colloid dispersions, and etcetera. It leads to concentration over-potential, limiting-current effect, membranes fouling, reduction of selectivity and productivity of the membrane processes, etc.

CP has been observed experimentally in micro/nano fluidic systems, for example in some studies where considerable current-induced enrichment/depletion in the concentration of charged fluorescent markers was directly observed close to micro/nano-interfaces (Kovarik, Zhou, & Jacobson, 2009; Zangle, Mani, & Santiago, 2009). Furthermore, nonlinear and time-dependent current voltage characteristics have also been observed, which can be interpreted in terms of the concentration-polarization phenomenon. (Kelly, Miller, & Timperman, 2009; Kim, Wang, Lee, Jang, & Han, 2007). This phenomenon as applied to micro/nano fluidic systems has also been considered theoretically in a number of recent publications (Postler, Slouka, Svoboda, Pribyl, & Snita, 2008; Yaroshchuk, Zholkovskiy, Pogodin, & Baulin, 2011; Zangle, Mani, & Santiago, 2010).

Some specific manifestations of CP in microfluidic systems have been studied. For example, the concentration “shock waves” which occur in current-polarized sub-micro-channels in contact with nano-channels have been predicted for the first time by (Mani, Zangle, & Santiago, 2009). In another publication (Zangle et al., 2010), the same authors considered the implications of depletion and enrichment “shocks” for the analyte pre-concentration via stacking and/or focusing. Several sample pre-concentration modes coupled to CP phenomena were also studied numerically by (Plecis, Nanteuil, Haghiri-Gosnet, & Chen, 2008) within the scope of 1D approach. (Strickland, Suss, Zangle, & Santiago, 2010) and (Suss, Mani, Zangle, & Santiago, 2011) studied the CP phenomena in the operation of nano-porous electroosmotic pumps and found the CP propagation to be important for their performance. The existence of moving sharp concentration “fronts” has also been predicted theoretically for current-polarized joined nano-/micro-systems with strong hydrodynamic dispersion in their micro-channel parts (Yaroshchuk et al., 2011).

According to the previous study (Licon Bernal et al., 2014), the overlap of a pressure driven flow with electroosmotic flow (Electroosmotic circulation, EOC) in micro-channels enhances considerably the hydrodynamic dispersion and results in a specific distribution of solutes in them. It was demonstrated that under conditions of a steady zero net flow (with zero cross-section average longitudinal velocity) the longitudinal profile of cross-section-averaged solute concentration is linear and the Taylor-Aris Dispersion theory (TAD) (Aris, 1956; Taylor, 1953) is approximately applicable locally within a major inner part of a long narrow channel. The applicability of the TAD to the description of the mass transport in narrow long channels under EOC has been the subject of some recent studies (Rubinstein & Zaltzman, 2013; Yaroshchuk et al., 2011). (Yaroshchuk et al., 2011) used a 1D approach to describe the distribution of an electrolyte in a micro-channel closed with a micro-/nano-interface, in order to show that the hydrodynamic-dispersion mechanism becomes effective in micro-channels sufficiently broad compared to the thickness of electrical double layer at its surfaces. On the contrary, the surface-conductance mechanism is responsible for the appearance of deionization “shocks” in sub-micro-channels, and hence those two mechanisms operate under very different conditions. Therefore one of them can be disregarded when considering the other. Rubinstein and Zaltzman (Rubinstein & Zaltzman, 2013) considered approximate analytical and numerical solutions of 2D convective-diffusion problem for a micro-channel with different boundary conditions at the channel ends to follow the breakdown of the Taylor–Aris dispersion mechanism with increasing circulation velocity.

The importance of EOC for microfluidics lies in the fact that it could be a way to reduce the CP near porous media used in microfluidic systems which results in the limiting and over-limiting current phenomena (Dydek et al., 2011; Yaroshchuk et al., 2011). To sum up, the studies of the transport mechanisms in microfluidic systems involving EOC are important for understanding the particularities of such phenomena as concentration polarization or concentration shocks and the role of hydrodynamic dispersion in these phenomena.

In this work we consider the steady-state distribution of an electrolyte species in a micro-channel under EOC with imposed different concentrations at the ends of the channel. This is a continuation of the previous study (Licon Bernal et al., 2014), where the transport of a non-electrolyte species under similar conditions was considered. Imposing different concentrations of electrolyte at the channel ends, we can be approaching the real situation of concentration polarization within the channel without the complex coupling between the local concentration at the boundary of ion-exchange material with electrolyte solution and the electric current passing though this boundary. Numerical simulations are

contrasted against the overall analytical description of the system. Furthermore, simple parametric relationships are derived to capture the principal features of the phenomena and the behavior of current vs voltage characteristics curves. One of the important aims of this study is to prove that the Taylor-Aris dispersion theory is approximately applicable locally, within the channel, irrespective of the inner conductivity gradients.

Formulation of the problem and governing equations

In the previous part of this study (Licon Bernal et al., 2014) we considered the convective-diffusion transport of a non-electrolyte in an open long channel with different fixed solute concentrations at the ends in presence of a buffer electrolyte, which's concentration is constant throughout the system. Due to the constant buffer electrolyte concentration the velocity of electroosmotic flow at the channel walls is not varying along the channel and is independent on the non-electrolyte distribution. Under such conditions, the hydrodynamics is decoupled from the solute transfer.

In the present study we consider the transport of an electrolyte whose concentration is varying along the channel. In this case, in contrast to the previous study the velocity of electroosmotic flow is not constant along the channel and is dependent on the local electrolyte concentration. Hence, the hydrodynamics is not decoupled from the solute transfer now and the consideration becomes more complicated. In addition, if the electroosmotic flow velocity varies along the channel then a transversal velocity component appears due to flow continuity. The transversal velocity influences the concentration distribution within the channel cross-sections, therefore, affecting the overall mechanism of the solute transfer. Nevertheless, as will be shown below, also in this case the Taylor-Aris dispersion theory appears to be approximately applicable locally within certain limits of the system parameters.

For the numerical description of the transport phenomena of the electrolyte inside a micro-channel, we will consider the steady state advection-diffusion and Navier-Stokes equations coupled with the electric current conservation law:

$$\nabla \cdot \left(- D \nabla C \right) + \mathbf{u} \cdot \nabla C = 0 \tag{1}$$

$$\rho \left(\mathbf{u} \cdot \nabla \right) \mathbf{u} = \nabla \cdot \left(\mu \nabla \mathbf{u} - P \right); \qquad \nabla \cdot \mathbf{u} = 0 \tag{2}$$

$$\nabla \cdot \boldsymbol{J} = 0; \qquad \boldsymbol{J} = \sigma \boldsymbol{E}; \qquad \boldsymbol{E} = -\nabla V \tag{3}$$

where D and C are the electrolyte diffusion coefficient and concentration, ρ and μ are the solution density and dynamic viscosity, P is the pressure, $\boldsymbol{u} = \begin{bmatrix} u_x \\ u_y \end{bmatrix}$ is the velocity vector,

$\nabla = \left[\frac{\partial}{\partial x} \quad \frac{\partial}{\partial y} \right]$ is the differential operator, *x* and *y* are the longitudinal and transverse coordinates, respectively, for a flat channel, $\boldsymbol{J} = \begin{bmatrix} j_x \\ j_y \end{bmatrix}$ and $\sigma = \alpha C$ are the local electric current density and conductivity, *α* is the proportionality constant of the conductivity to the concentration, and *E* and *V* are the local electric field strength and potential.

In order to define the boundary conditions for such problem, first different constant concentrations at the both channel ends and zero flux condition at the walls are set as:

$$C(0,y) = C_0; \quad C(L,y) = C_L; \quad \mathbf{n} \cdot \left(-D\nabla C(x,\pm h) + \mathbf{u}C(x,\pm h) \right) = 0 \tag{4}$$

where *h* and *L* are the half-thickness and the length of the channel (*h* << *L*).

The hydrodynamic boundary conditions at the edges of the channels are defined using the assumption of zero normal stress ($\frac{\partial u_x}{\partial x} = 0$), which is compatible with the supposal of a channel connected to a big reservoir (Panton, 2013), and the exact compensation of Poiseuille and electroosmotic flows (Licon Bernal et al., 2014):

$$u_x(0,y) = \frac{u_{eo}(0)}{2}\left(\frac{3y^2}{h^2} - 1 \right) \text{ and } u_y(0,y) = 0 \tag{5a}$$

$$u_x(L,y) = \frac{u_{eo}(L)}{2}\left(\frac{3y^2}{h^2} - 1 \right) \text{ and } u_y(L,y) = 0 \tag{5b}$$

The y-component condition follows from the conditions $\frac{\partial u_x}{\partial x} = 0$ and the continuity equation ($\frac{\partial u_x}{\partial x} = -\frac{\partial u_y}{\partial y}$). So defined boundary conditions reflect the fact that there are no any erupt changes in the flow patterns at the two ends of the microchannel (Lee, Ren, & Li, 2005).

Additionally, the condition of zero total volume flux must be satisfied at the ends of the channel by setting the cross-sectional averaged velocity equal to zero:

$$\bar{u}_x(0) = \frac{1}{2h}\int_{-h}^{h} u_x(0,y)dy = \bar{u}_x(L) = 0 \tag{5c}$$

The slip condition holds for the velocity at the channel walls, defined as the velocity of the electroosmotic flow found with the Helmholtz-Smoluchowski equation

$$u_{eo}(x) = u_x(x,\pm h) = -\frac{\varepsilon\varepsilon_0\zeta}{\mu} E_x(x,\pm h) \tag{6}$$

where ε is dielectric permittivity, ε0 is permittivity of vacuum, and ζ is the zeta-potential at the walls. The electroosmotic flow superimposed with the pressure-driven flow produce the characteristic flow field of electroosmotic circulation. Similarly to the previous study we will assume here that the electroosmotic flow and the pressure-driven flow compensate each other completely giving zero total volume flow through the channel (see Eq.(5)).

Although the definition of the boundary condition for the hydrodynamics is complicated, the concentration profile inside the channel is not appreciably changed using different boundary conditions at the channel ends due to the constant concentration set on the same boundaries.

Finally, the current density is set constant at the cannel edges, while the channel walls are considered to be impermeable

$$\boldsymbol{n}\cdot\boldsymbol{J}(0,y)=-\boldsymbol{n}\cdot\boldsymbol{J}(L,y)=J_0;\qquad \boldsymbol{n}\cdot\boldsymbol{J}(x,\pm h)=0 \tag{7}$$

We will assume here that electro-neutrality condition holds everywhere within the electrolyte solution, except of infinitely thin layers at the channel walls. Eqs.(3) and (7) show that the total electric current through each channel cross-section should be constant.

Though we consider channel walls with constant zeta-potential, the electroosmotic flow velocity varies along the channel because of the varying solution conductivity (due to the changing electrolyte concentration). Neglecting the variation of the electric field in a cross-section (which is small according to calculations, see below in Subsection 4.2) we can write approximately $E_x(x,\pm h)=\dfrac{I}{\alpha\overline{C}(x)}$, where *I* is the average current density and $\overline{C}(x)$ is the average concentration. Then, according to Eq.(6), the electroosmotic flow velocity should be inversely proportional to the electrolyte concentration

$$u_{eo}(x)=\frac{\chi}{\overline{C}(x)} \tag{8}$$

where $\chi=-\dfrac{\varepsilon\varepsilon_0\zeta I}{\mu\alpha}$ is the proportionality coefficient. The direction of the electroosmotic flow depends on the direction of the current and the sign of zeta-potential at the walls.

A 2D model has been solved by Finite Element method (FEM) with COMSOL Multiphysics 4.2a to describe the concentration distribution of a salt (KCl) dissolved in water inside a flat micro-channel. During the numerical simulation, different values of the electric current (*I*) passing through the channel have been evaluated, with the purpose of investigating the

coupling between velocity distribution and the transport phenomena. The local conductivity, σ, was calculated according to ideal solution approximation with the respective diffusion coefficients for the ions (K^+ and Cl^-).

The first step was to declare the domain as a rectangle of the length *L* and the height two times *h* with a displacement in the y coordinate of *–h*. A fixed value of *h* = 100 µm was used for all the calculations, while the channel lengths (*L*) was varied. The concentrations at the entrances of the channel were set to C_0 = 1 mol/m^3 and C_L = 10 mol/m^3. In order to see the effect of the concentration ratio C_L/C_0, C_0 = 0.01 mol/m^3 was studied too. Then a free triangular mesh was created with a refinement on the walls of the micro-channel with a minimum element size of 1 micron. The equations were solved with the parallel direct linear solver (PARDISO) with a relative tolerance of 0.001.

Results

Electrolyte concentration distribution within the micro-channel

The numerical solutions for the electrolyte distribution under the conditions of EOC in a micro-channel and the corresponding velocity field are shown in Figure A1. It is noticed that the local magnitude of the velocity at the walls is inversely proportional to the electrolyte concentration. Therefore the local velocity magnitude is varying from one cross-section to other, however, preserving the same characteristic shape within all cross-sections, which is a superposition of an electroosmotic and a counter-pressure driven profiles with zero cross-section average velocity. Such velocity field gives rise to a transversal non-uniformity in the concentration distribution which will be studied under several conditions below.

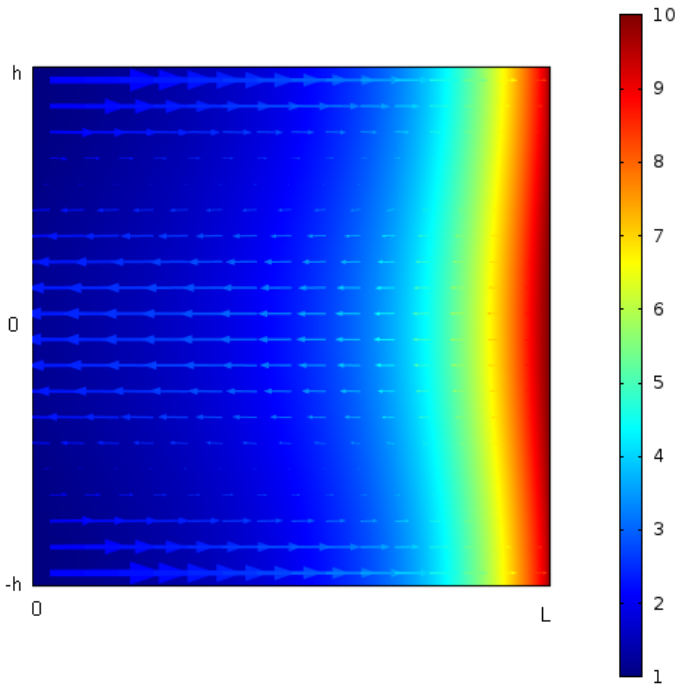

Figure A1. Velocity field (arrows) and electrolyte concentration, mol/m^3 (color), in a channel of 4 mm length and half-height h = 100 μm for the current density I = 250 A/m^2 ($u_{eo} > 0$).

Figure A2 shows how the averaged concentration profile depends on the current density. A non-linear, concave, shape can be distinguished for all the curves and this non-linearity becomes more pronounced with increasing current density. The non-linear shape of the concentration profiles is a consequence of non-uniformity of electroosmotic velocity. The velocity is higher in the left part of the channel, and, therefore, the dispersion coefficient $D_T = D \cdot \left(1 + \frac{2}{105}\frac{h^2 u_{eo}^2}{D^2}\right)$ is larger here. However, this is compensated by a smaller concentration gradient in this part of the channel. In contrast, on the right side the velocity and the dispersion coefficient are smaller, but the concentration gradient is larger. This provides the necessary continuity of the solute flux in all parts of the channel under steady-state flow conditions, according to Eq.(19).

On the side of more diluted solution the presence of a small concentration “jump” can be noticed (Figure A2). On the side of more concentrated solution the similar “jump” is much less pronounced. With increasing circulation rate the “jumps” of the cross-section average concentration at the borders are increasing. Simultaneously, the size of the boundary layers also increases. The similar boundary layers are observed also by the transfer of a non-electrolyte in presence of a buffer electrolyte considered in Part I of this study.

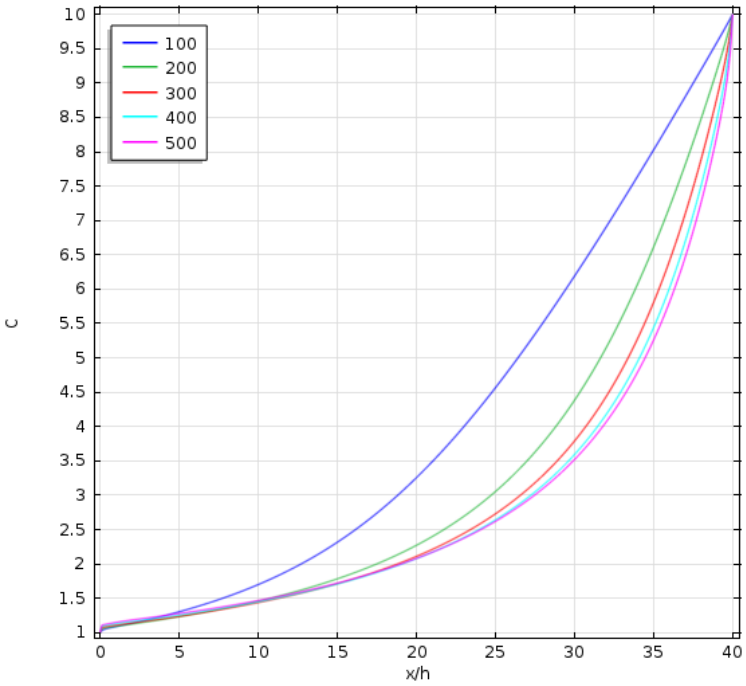

Figure A2. Averaged concentration profiles in a channel of 4 mm length and half-height h = 100 μm for different values of current density: 100, 200, 300, 400, 500 A/m^2 (u_{eo} > 0).

The electric field is proportional to current density and inversely proportional to conductivity, therefore, according to Eq.(6), the electroosmotic velocity is inversely proportional to the concentration. On Figure A3 the reciprocal concentration profiles are shown for the same current densities, as in Figure A1, and it can be noted that for higher current densities, used for these simulations, the reciprocal concentration profile becomes close to linear inside the channel. Such transformation of the concentration profile with increasing current density is in agreement with the approximate analytical solution presented above (cf. Eq.(20)), and this is an indication that the Taylor-Aris approach is approximately applicable to the description of steady state transport of an electrolyte in this system. However, there are boundary zones at the edges of the channel where this behavior is loosed, as it was also in for the system with non-electrolytes transfer (Part I).

In order to compare these two systems, longitudinal cross-section profiles along the channel for three different heights (y = *0*, $h/\sqrt{3}$ and h) are plotted in Figure A4. Different slopes for these three cases are observed, what is explained by the difference in local conductivities. In contrast, for the system with transfer of non-electrolytes the profiles were running parallel for the same longitudinal cross-sections due to the constant buffer electrolyte concentration and constant conductivity in the channel.

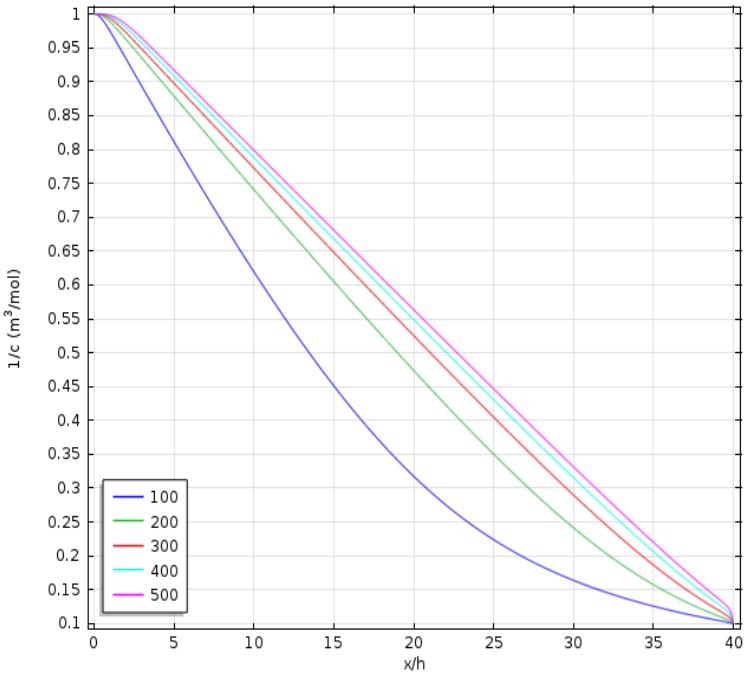

Figure A3. Reciprocal local concentration profiles along the channel wall for different values of current density (in A/m^2) for the channel of 4 mm length and half-height h = 100 μm (u_{eo} > 0).

Since intensity of convection is dependent on the electric field, the boundary zone near the channel edge with more diluted solution ($x = 0$) is more pronounced than that on the opposite side. Additionally, as in the case of non-electrolytes, the length of this zone strongly varies with the transversal coordinate, y. The boundary zone is very small in those parts of the cross-section where the solutions leave the channel (at the side with diluted solution for $u_{eo} > 0$ this is near the middle horizontal plane, $y \approx 0$, and at the opposite side - near the walls, $y \approx \pm h$), and it is much larger at the locations, where the solutions enter the channel ($y \approx \pm h$ at the side with diluted solution and $y \approx 0$ at the opposite side).

Figure A5 is a contour plot of the reciprocal concentration. It shows the evolution of the profiles shape from the constant concentrations at the edges to the Taylor-Aris type profiles in the inner part of the channel.

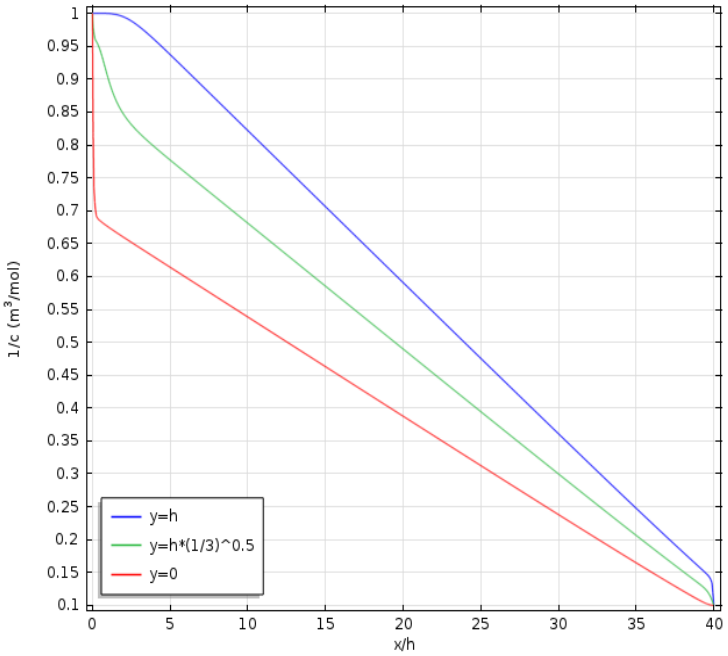

Figure A4. Reciprocal local concentrations profiles along the channel for different longitudinal cross-sections at the current density of 800 A/m^2 for the channel of 4 mm length and half-height h = 100 μm (u_{eo} > 0).

On the left channel side (close to $x = 0$) in vicinity of the walls, there are extended zones where the concentration almost does not change, remaining practically the same as at the edge. These zones arise due to protrusions of the external solution near the walls. The similar protrusion zone appears also on the right side of the channel ($x = L$), but in vicinity of the middle plane ($y \approx 0$). Such protrusions of the external solutions result in distortions of the transversal concentration profiles compared to those established within the inner parts of the channel away from its ends. At the internal edges of these region ($x = x_s$ and $x = 1\text{-}x_m$) the concentration profiles transform gradually to the profiles corresponding to the TAD theory. The same effects within the entrance zones of the channel were observed also in the case of non-electrolytes transfer, considered in the Part I of this study.

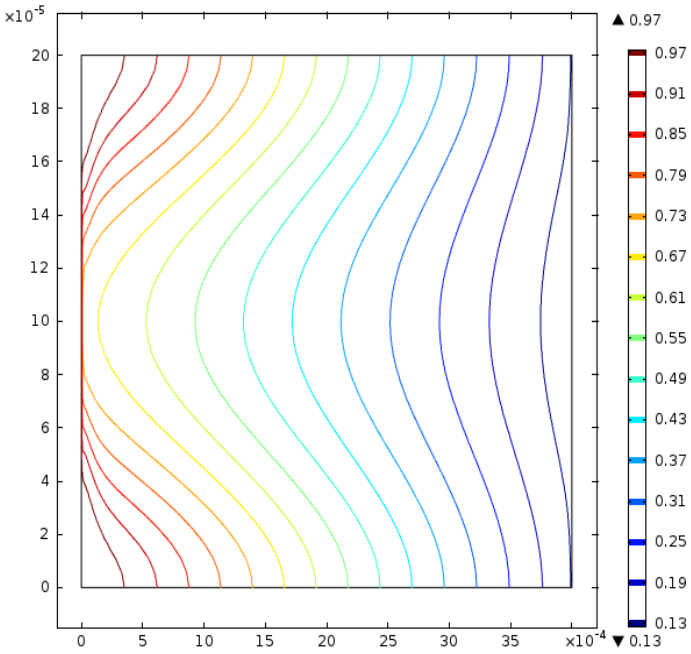

Figure A5. Contour graph showing the distribution of the reciprocal concentration within the channel at the current density of 800 A/m^2 for the channel of 4 mm length and half-height h = 100 μm (the scale for the distance in x and y directions is in m, $u_{eo} > 0$).

Electric field distribution

The ratio of the transversal and longitudinal electric field components is shown on Figure A6. It is seen that inside the channel the transversal component of the field is negligible when comparing it against the longitudinal. They become of the same order of magnitude only very close to the edges of the channel. The one-dimensionality of the field reflects a close to uniform local conductivity within the cross-sections of the internal part of the channel what is a consequence of small deviations of the concentration from average. Such almost uniform local conductivity allows assuming the inverse proportionality of the electroosmotic velocity to the average concentration, $u_{eo} \approx \chi / \overline{C}$ (see Eq. (8)). As expected, calculated numerically values $\chi \approx u_{eo}\overline{C}$ are practically constant, for example, this value is 4.63*10^{-4} mol/(m^2*s) for 100 A/m^2 and C_L/C_0 = 100, varying along the channel by less than 0.1% (out of the entrance boundary layers). Moreover it shows a linear dependence with the current density.

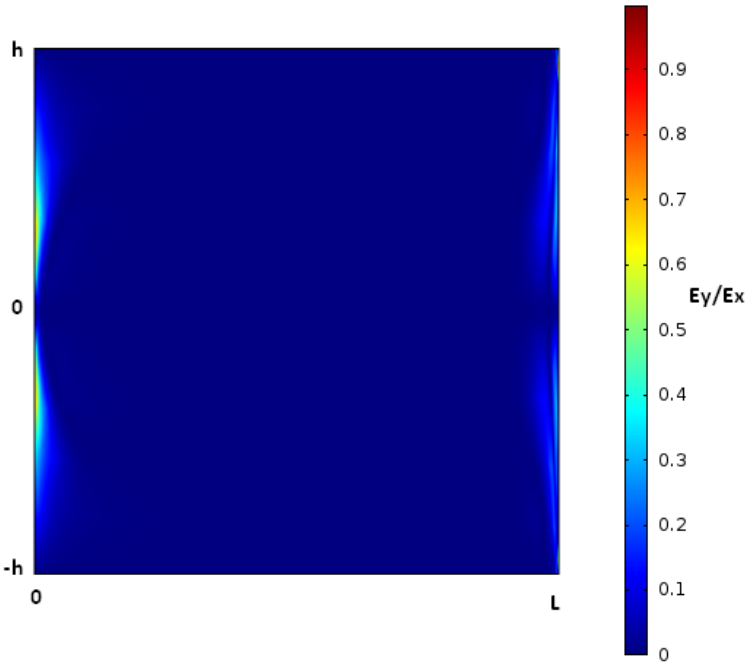

Figure A6. Ratio of the transversal and longitudinal electric field components (E_y/E_x) at 800 A/m^2 of current density inside the micro-channel of 4 mm length and 100 μm of half-height with a concentration ratio C_L/C_0 = 100 ($u_{eo} > 0$).

Hydrodynamics

The profile of the absolute value of longitudinal velocity in the middle cross-section ($x = L/2$) of the channel is presented in Figure A7a. This profile is the result of the superposition of two, a parabolic (pressure-driven) and an electroosmotic (plug) flow. The velocity is zero at $\tilde{y} = \pm 1/\sqrt{3}$. The same points correspond to the locations of the largest absolute values of the transversal component of the velocity arising due to flow continuity, Figure A7b.

Due to changes in the conductivity along the channel, the magnitude of the profile variation across the channel changes depending on the local average concentration of the electrolyte, though the shape of the profile remains the same (except of the entrance boundary layers). In Figure 5 the size of the arrows represents the relative magnitude of the velocity for different cross sections, showing the variation of the velocity along the channel. A couple of lines in this figure represent the points within the cross-sections where the direction of the liquid flow changes to the opposite and where the transversal component is the largest.

The intensity of convection is larger near the left edge ($x = 0$) than in the rest of the channel because the electrolyte concentration is the smallest here. Near the edge the direction of the arrows is not plane parallel but has a trend to deviate to the middle of the

channel because the concentration distribution within the boundary layers is strongly different from the major part of the channel. A velocity distribution near the entrances depends on the particular boundary conditions set for the velocity at the edges. Hydrodynamic boundary layers should arise at the entrances, within which the velocity profiles transform from those at the edges to those corresponding to the TAD approximation, established inside the channel.

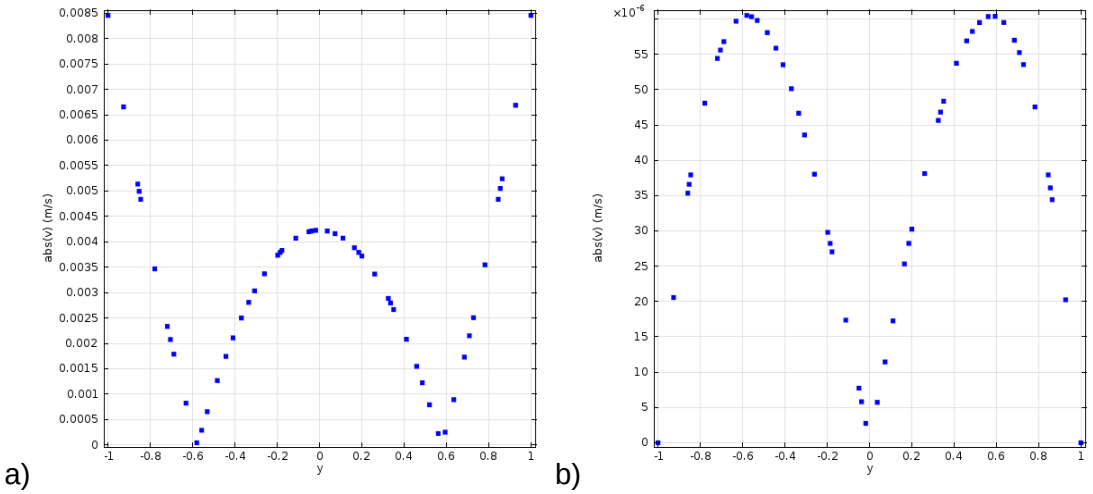

a) b)

Figure A7. Velocity profile developed under the current density 800 A/m^2 at the middle cross-section of the channel ($x = L/2$) for a) x-component and b) y-component; channel length L = 4 mm, half-height h = 100 μm, concentration ratio C_L/C_0 = 100 ($u_{eo} > 0$).

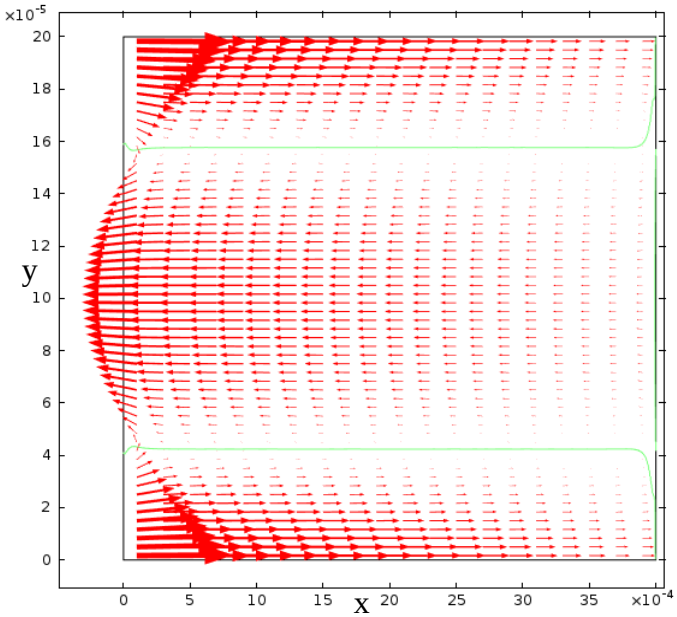

Figure A8. Velocity field within the channel under 100 A/m^2 of current density; channel length L = 4 mm, half-height h = 100 μm, concentration ratio C_L/C_0 = 100 ($u_{eo} > 0$). The green lines correspond to the positions of zero longitudinal velocity.

Applicability of Taylor-Aris approach

As it has been shown above, for the considered here system the Taylor-Aris approach is valid as a first-order approximation only, because the contribution of the transversal convection leads to deviations from the behavior expected according to this approach. To evaluate the applicability of the Taylor-Aris approximation we need to have certain quantitative criterion. As such criterion we can consider here the deviation from unity of the ratio of the actual solute flux, calculated numerically ($-D\frac{d\overline{C}}{dx}+\overline{u_x C}$), to that given by the Taylor-Aris approximation

$$R=\frac{-D\frac{d\overline{C}}{dx}+\overline{u_x C}}{-D\left(1+\frac{2}{105}\frac{h^2u_{eo}^2}{D^2}\right)\frac{d\overline{C}}{dx}}=\frac{1}{1+\frac{2}{105}\frac{h^2u_{eo}^2}{D^2}}\left(1-\frac{\overline{u_x C}}{D\frac{d\overline{C}}{dx}}\right) \tag{9}$$

Deviation of the numerically calculated parameter *R* from unity can be a useful criterion to identify the particular conditions and regions of the channel, for which the transport phenomena can be interpreted in terms of TAD mechanism. In Figure A9, the profiles of the parameter *R* are presented for a channel of 4 mm length and 100 μm half-height. The effect of the current density (100, 200, 300, 400, and 500 A/m^2) is evaluated for a concentration ratio of 10 for two directions of electroosmotic velocity: Figure A9a shows the case where the electroosmosis is directed from *x = 0* to *x = L*, whereas Figure A9b corresponds to oppositely directed electroosmotic flow. Both cases show small deviations from the TAD theory in the inner part of the channel and strongly increasing deviations in the small regions near to the channel ends. Furthermore at relatively low current densities, the deviations from TAD analysis are lower and they are increasing with the current. Moreover, by comparing the two graphs a clear dependence on the current direction is evident. Although they look as to have a mirror-like symmetry, the deviation is larger for the case of Figure A9a.

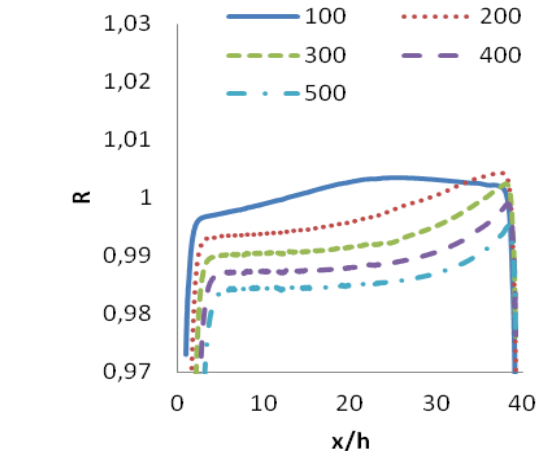

a)

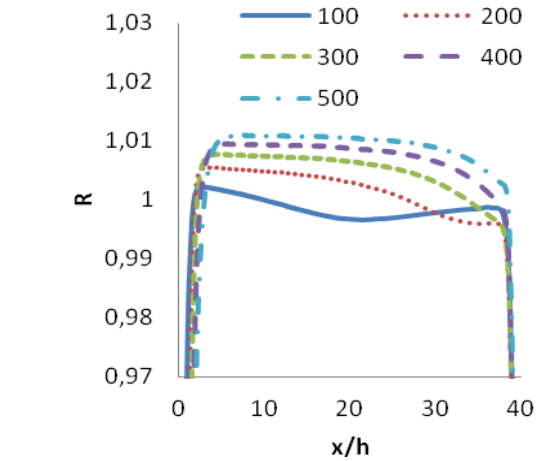

b)

Figure A9. Deviation from Taylor-Aris theory, represented by the parameter *R*, for the velocity of electroosmosis directed: a) from *x = 0* to *x = L,* and b) in the opposite direction, along the channel of 4 mm length and half-height *h* = 100 μm for different values of the current density (100, 200, 300, 400, and 500 A/m^2) and the concentration ratio of 10.

Approximate parametric description

Transition boundary layers are formed near the channel edges where the concentration profiles transform from the constant concentrations set at the channel borders (*x = 0, L*) to those characteristic of the TAD approximation at the internal face of these boundary layers (*x = x_s* and *x = L - x_m*). Similarly to the case of non-electrolyte solutions, in order to define the length of this entrance zone, x_s, we can extrapolate the linear inner part of the local reciprocal concentration profile at the wall (for the in-flowing solution) until it reaches the value $1/C_0$ (see Figure A3), corresponding to the boundary condition. The results obtained with this procedure are presented in Table A1. The length of the entrance zone at the opposite end of the channel, x_m, can be obtained in a similar way. In view of its weak contribution and according to the numerical results, we will

assume the entrance zone at the channel edge with higher concentration to be infinitely thin, x_m = 0, (but we will take into account the average concentration "jump" within this entrance zone, see below).

Table A1. Normalized size of the entrance zone, x_s/h, for different values of current density, I, and aspect ratio, L/h, and for a concentration ratio C_L/C_0 = 10.

	L/h			
I (A/m²)	**10**	**20**	**40**	**60**
100	0.490	0.477	0.305	0.252
200	0.863	0.697	0.508	0.421
300	1.183	0.962	0.869	0.618
400	1.554	1.290	1.151	0.980
500	1.863	1.630	1.433	1.256
600	2.130	1.934	1.715	1.499
700	2.365	2.212	1.997	1.741
800	2.580	2.469	2.279	1.974

Having the lengths of the entrance zone, x_s, for various current densities, we can obtain the average concentrations at the internal sides of the boundary layers $C_1 = \overline{C}(\tilde{x}_s)$ and $C_2 = \overline{C}(1-\tilde{x}_m)$, which give us immediately the respective concentration "jumps" at the borders (C_1 - C_0 and C_L - C_2). These concentrations are determined as a solution of a set of two equations for two unknowns, C_1 and C_2.

$$C_1 = C_0 - \frac{F}{15\left(\frac{L}{h}-\frac{x_S}{h}\right)} \frac{\left[\left(C_1-C_2\right)+\frac{2F^2}{105}\left(\frac{1}{C_2}-\frac{1}{C_1}\right)\right]}{C_1+\frac{2F^2}{105}\frac{1}{C_1}} \tag{10}$$

$$C_2 = C_L + \frac{7F}{120\left(\frac{L}{h}-\frac{x_S}{h}\right)} \frac{\left[\left(C_1-C_2\right)+\frac{2F^2}{105}\left(\frac{1}{C_2}-\frac{1}{C_1}\right)\right]}{C_2+\frac{2F^2}{105}\frac{1}{C_2}} \tag{11}$$

Where $C_1 = \overline{C}(\tilde{x}_s)$, $C_2 = \overline{C}(1-\tilde{x}_m)$, $\chi = -\frac{\varepsilon\varepsilon_0\zeta I}{\mu\alpha}$ and $F = \frac{h\chi}{D}$

Once those concentrations are determined, they can be used to obtain parametric equations for description of the averaged concentration profile in the inner part of the channel by using the parameter x_s/h, numerically obtained (the parameter x_m/h can be also calculated)

$$\overline{C}(x)=\frac{1}{2}\left(\tilde{Q}(1-\tilde{x}_m-\tilde{x})+C_2-\frac{2F^2}{105}\frac{1}{C_2}\right)+\sqrt{\frac{1}{4}\left(\tilde{Q}(1-\tilde{x}_m-\tilde{x})+C_2-\frac{2F^2}{105}\frac{1}{C_2}\right)^2+\frac{2F^2}{105}} \quad (12)$$

$$\tilde{Q}=\frac{1}{1-\tilde{x}_S-\tilde{x}_m}\left[(C_1-C_2)+\frac{2F^2}{105}\left(\frac{1}{C_2}-\frac{1}{C_1}\right)\right] \quad (13)$$

In Eqs.(10)-(13) the parameter F combines the physical properties of the system.

From the data in Figure A10 it is seen that the concentrations approximately obtained at the left-hand side of the channel, C_1, are slightly higher than C_0 whereas those for the right-hand side, C_2, are smaller than C_L. With increasing current density the both concentration "jumps", C_1 - C_0 and C_L - C_2, are increasing. Even though the entrance zone at the channel edge with higher concentration was not taken into account (x_m = 0), a good agreement is observed between the results of both calculation methods. The agreement is better in the case of larger aspect ratios (L/h) where the entrance zones have a weaker contribution to deviation of the system behavior from that expected according to the TAD formalism.

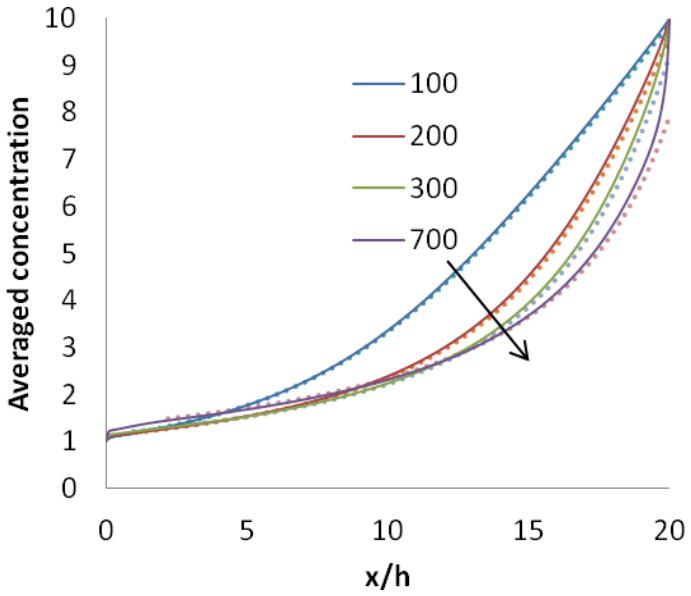

a)

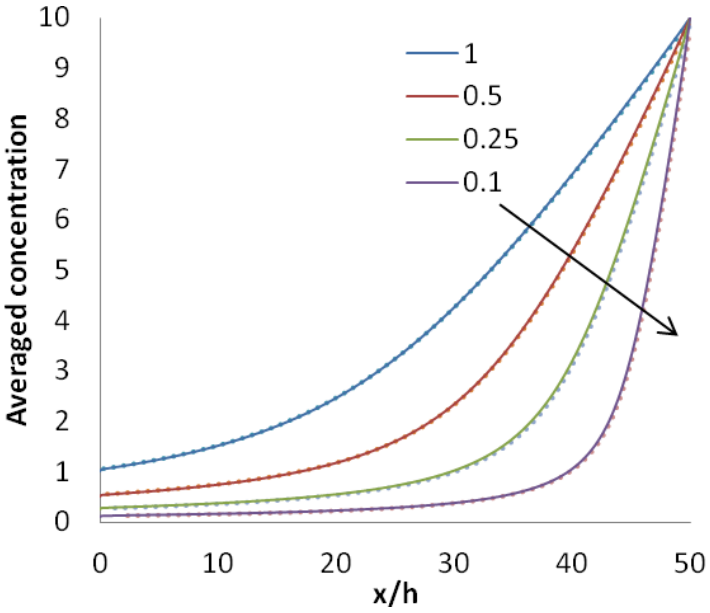

b)

Figure A10. Comparison between the cross-sectional averaged concentration profiles calculated numerically and the respective profiles obtained analytically (Eqs.(32)-(35)) for: a) aspect ratio L/h = 20, concentration ratio C_L/C_0 = 10 and different current densities (100, 200, 300 and 700 A/m^2); b) aspect ratio L/h = 50, current density 100 A/m^2, and different values of the lower concentration (C_0 = 1, 0.5, 0.25 and 0.1).

Current vs voltage characteristic curves

According to these results, the approximate parameterization procedure described in the previous subsection can be used to obtain the current as a function of voltage for different conditions. This can be done by using the next approximate expression:

$$V = \int_0^L \frac{I}{\alpha \overline{C}(x)} dx \qquad (14)$$

A good agreement between the analytical and numerical procedures is found in a rather large range of currents and voltages for the three different aspect ratios presented in Figure A11. A larger range of current-voltage can be achieved with good applicability of the approximate method when longer channels are being used.

The current vs voltage curves have a characteristic shape with a plateau resembling a limiting current followed by a portion with faster current increase ("over-limiting" current). Such shape of the curves is explained by the changes in concentration distribution within the channel. With increasing current the velocity of electroosmotic flow increases what leads to formation of concave concentration profiles, as shown in Figures A2 and A11. Hence the local conductivity in all parts of the channel decreases and, accordingly, the applied voltage increases. Therefore the current increases with the voltage slower. However, for larger currents the concentration profile within the channel

approaches its limiting shape, characterized by a linear reciprocal concentrations profile (Eq.(29)), and the concentration cannot decrease further. Simultaneously, the concentration "jump" at the left-hand side of the channel (C_1 - C_0) gradually increases, as discussed above. This leads to an increase of the local conductivity in the left part of the channel, i.e. in the part where it is the smallest. Therefore, the differential resistance of the channel decreases and one observes a faster current increase after the plateau.

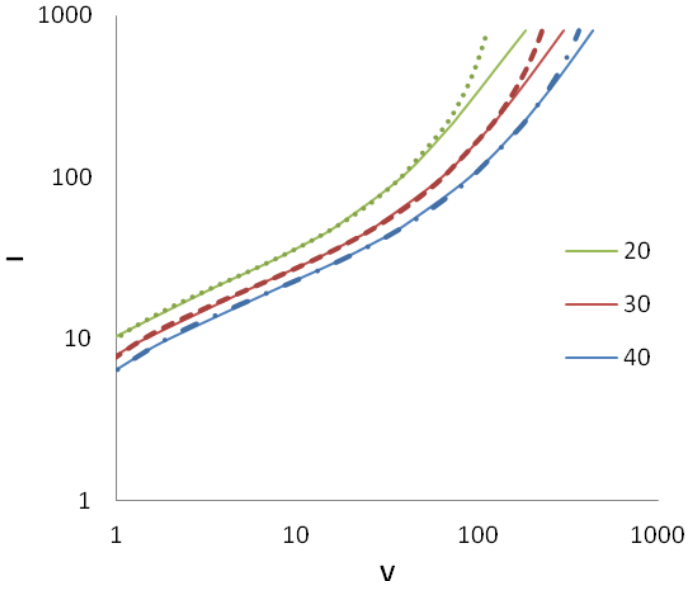

Figure A11. Current vs voltage curves for different aspect ratios (L/h = 20, 30 and 40) with a concentration ratio C_L/C_0 = 100. Dashed lines belong to the analytical procedure and solid lines are for the numerical.

Conclusions

The results of numerical simulations and approximate analytical solution show that the concentration distribution within a major part of a long channel under conditions of electroosmotic circulation are in a good agreement with that predicted by the TAD formalism with the exception of only two boundary layers formed at the edges. Because of varying electroosmotic flow velocity along the channel the TAD approximation is approximately applicable locally within the internal channel cross-sections and the dispersion coefficient is not a constant but is a function of the local Péclet number.

Due to the condition of constant concentrations imposed at the channel edges, the concentration profiles are distorted from the Taylor-like shape within the boundary layers formed at the edges. This results in appearance of “jumps” of average concentration at the channel edges. The lengths of the entrance zones with distorted concentration profiles ($x_{s,m}$) are controlled by the local concentration, electrical current density (electric field or

local Peclet number) and the height of the channel. They are almost independent of the channel length until they increase to become comparable with it.

These entrance zones control the magnitude of "jumps" of average concentration at the channel edges and, thus, the inner concentration profile. With increasing Pe, the external solutions from the reservoirs penetrate deeper into the channel and deform stronger the transversal concentration profiles, producing larger deviations from the TAD approximation in a larger portion of the channel. These features are confirmed by both numerical and analytical calculations. Minor deviations are observed between them in a rather wide range of electrical current densities, aspect ratios and concentration ratios.

An approximate parametric description can be proposed which simplify the calculations of the concentration distribution within the channel and the current-voltage characteristics of the system. Such parametric description can be important for practical use in analysis of experimental data on electroosmotic circulation and concentration polarization in long micro-channels.

Nomenclature:

c: Concentration, mol/m^3.
D: Diffusion coefficient, 2e-9 m^2/s.
h: half height, 0.0001 m.
I: Current density, A/m^2.
L: Channel length, m.
Z_p: Zeta potential, 0.1V.
α: Conductivity coefficient, .015278 $(S*m^2)/mol$.
$\varepsilon\varepsilon_o$: Permittivity of the media, 80*8.8541e-12 F/m
η: Dynamic viscosity, 1e-3 Pa*s.
σ: Conductivity, S/m.

References

Aris, R. (1956). On the dispersion of a solute in a fluid flowing through a tube. *Proc. R. Soc. London*, *235*, 67–77.

Dydek, E. V., Zaltzman, B., Rubinstein, I., Deng, D. S., Mani, A., & Bazant, M. Z. (2011). Overlimiting Current in a Microchannel. *Physical Review Letters*, *107*(11), 118301. doi:10.1103/PhysRevLett.107.118301

Kelly, K. C., Miller, S. A., & Timperman, A. T. (2009). Investigation of Zone Migration in a Current Rectifying Nanofluldic/Microfluidic Analyte Concentrator. *Analytical Chemistry*, *81*(2), 732–738. doi:10.1021/ac802209e

Kim, S. J., Wang, Y.-C., Lee, J. H., Jang, H., & Han, J. (2007). Concentration polarization and nonlinear electrokinetic flow near a nanofluidic channel. *Physical Review Letters*, *99*(4), 44501. doi:10.1103/PhysRevLett.99.044501

Kovarik, M. L., Zhou, K., & Jacobson, S. C. (2009). Effect of Conical Nanopore Diameter on Ion Current Rectification. *Journal of Physical Chemistry B*, *113*(49), 15960–15966. doi:10.1021/jp9076189

Lee, J. S. H., Ren, C. L., & Li, D. (2005). Effects of surface heterogeneity on flow circulation in electroosmotic flow in microchannels. *Analytica Chimica Acta*, *530*(2), 273–282. doi:10.1016/j.aca.2004.09.026

Licon Bernal, E. E., Kovalchuk, V. I., Zholkovskiy, E. K., & Yaroshchuk, A. (2014). Hydrodynamic dispersion in long microchannels under conditions of electroosmotic circulation. I. Non-electrolytes. *Microfluidics and Nanofluidics*. doi:10.1007/s10404-014-1506-8

Mani, A., Zangle, T. a, & Santiago, J. G. (2009). On the propagation of concentration polarization from microchannel-nanochannel interfaces. Part I: Analytical model and characteristic analysis. *Langmuir : The ACS Journal of Surfaces and Colloids*, *25*(6), 3898–908. doi:10.1021/la803317p

Panton, R. L. (2013). *Incompressible Flow* (p. 912). John Wiley & Sons.

Plecis, A., Nanteuil, C., Haghiri-Gosnet, A.-M., & Chen, Y. (2008). Electropreconcentration with charge-selective nanochannels. *Analytical Chemistry*, *80*(24), 9542–50. doi:10.1021/ac8017907

Postler, T., Slouka, Z., Svoboda, M., Pribyl, M., & Snita, D. (2008). Parametrical studies of electroosmotic transport characteristics in submicrometer channels. *Journal of Colloid and Interface Science*, *320*(1), 321–332. doi:10.1016/j.jcis.2007.10.056

Rubinstein, I., & Zaltzman, B. (2013). Convective diffusive mixing in concentration polarization: from Taylor dispersion to surface convection. *Journal of Fluid Mechanics*, *728*, 239–278. doi:10.1017/jfm.2013.276

Strickland, D. G., Suss, M. E., Zangle, T. a., & Santiago, J. G. (2010). Evidence shows concentration polarization and its propagation can be key factors determining electroosmotic pump performance. *Sensors and Actuators B: Chemical*, *143*(2), 795–798. doi:10.1016/j.snb.2009.10.005

Suss, M. E., Mani, A., Zangle, T. A., & Santiago, J. G. (2011). Electroosmotic pump performance is affected by concentration polarizations of both electrodes and pump. *Sensors and Actuators A-Physical*, *165*(2), 310–315. doi:10.1016/j.sna.2010.10.002

Taylor, G. I. (1953). Dispersion of soluble matter in solvent flowing slowly through a tube. *Proc. R. Soc. London*, *219*, 186–203.

Yaroshchuk, A., Zholkovskiy, E., Pogodin, S., & Baulin, V. (2011). Coupled Concentration Polarization and Electroosmotic Circulation near Micro/Nanointerfaces: Taylor-Aris Model of Hydrodynamic Dispersion and Limits of Its Applicability. *Langmuir*, *27*(18), 11710–11721. doi:10.1021/la201354s

Zangle, T. a, Mani, A., & Santiago, J. G. (2009). On the propagation of concentration polarization from microchannel-nanochannel interfaces. Part II: Numerical and experimental study. *Langmuir : The ACS Journal of Surfaces and Colloids*, *25*(6), 3909–16. doi:10.1021/la803318e

Zangle, T. a, Mani, A., & Santiago, J. G. (2010). Theory and experiments of concentration polarization and ion focusing at microchannel and nanochannel interfaces. *Chemical Society Reviews*, *39*(3), 1014–35. doi:10.1039/b902074h

Publications

ATTENTION ¡

Pages 76-139 of the thesis contain 5 publications listed below, which are available on the website of the respective publishers

1. **Licon Bernal, E.E.; Kovalchuk, V.I.; Zholkovskiy, E.K.; Yaroshchuk, A.** *Hydrodynamic dispersion in long microchannels under conditions of electroosmotic circulation*. I. Non-electrolytes. Microfluidics and Nanofluidics 2014, p. 1-16 DOI 10.1007/s10404-014-1506-8 http://link.springer.com/article/10.1007%2Fs10404-014-1506-8#

2. **Yaroshchuk, A., Licon Bernal, E.E.; Luxbacher**, T. *Electrokinetics in undeveloped flows*. Journal of Colloid and Interface Science, vol 410, 2013, p. 195–201. doi:10.1016/j.jcis.2013.08.021 http://www.sciencedirect.com/science/article/pii/S0021979713007674

3. **Yaroshchuk, A., Bruening, M.L., Licon Bernal**, **E.E**. S*olution-Diffusion–Electro-Migration model and its uses for analysis of nanofiltration, pressure-retarded osmosis and forward osmosis in multi-ionic solutions.* Journal of Membrane Science vol 447, 2013, p. 463–476 Doi:10.1016/j.memsci.2013.07.047 http://www.sciencedirect.com/science/article/pii/S0376738813006236

4. **Licon Bernal, E.E.; Casas, S., Alcaraz, A., Cortina, J.L., Valderrama, C**. *Ammonia Removal from Water by Liquid-Liquid Membrane Contactor under Closed Loop Regime.* Excerpt from the Proceeding of the 2012 COMSOL Conference in Milan, p. 1-7. http://www.comsol.com/paper/download/152377/licon_paper.pdf

5. **Licon Bernal, E.E. , Reiga, M., Villanova, P., Valderrama, C., Gibert, O., Cortina, J.L** *Ammonium removal by liquid–liquid membrane contactors in water purification process for hydrogen production.* Desalination and Water Treatment, 2014, p. 1-10. DOI: 10.1080/19443994.2014.974216 http://www.tandfonline.com/doi/abs/10.1080/19443994.2014.974216?journalCode=tdwt20#.VSvbXeHXvhl